THE PLANT CELL

The Plant Cell, 2024, **36**, 3260–3276

https://doi.org/10.1093/plcell/koae183
Advance access publication 26 June 2024
Research Article

Bioengineering secreted proteases converts divergent Rcr3 orthologs and paralogs into extracellular immune co-receptors

Jiorgos Kourelis,[1,2,†] Mariana Schuster,[1,‡] Fatih Demir,[3,§] Oliver Mattinson,[1] Sonja Krauter,[1] Parvinderdeep S. Kahlon,[1,‖] Ruby O'Grady,[1] Samantha Royston,[1] Ana Lucía Bravo-Cazar,[1] Brian C. Mooney,[1] Pitter F. Huesgen,[3,¶] Sophien Kamoun,[2] and Renier A.L. van der Hoorn[1,*]

[1]The Plant Chemetics Laboratory, Department of Biology, University of Oxford, South Parks Road, OX1 3RB Oxford, UK
[2]The Sainsbury Laboratory, Norwich Research Park, NR4 7UH, Norwich, UK
[3]Central Institute for Engineering, Department of Electronics and Analytics (ZEA), Analytics (ZEA-3), Research Centre Jülich, Wilhelm-Johnen-Str., 52428 Jülich, Germany
*Author for correspondence: renier.vanderhoorn@biology.ox.ac.uk (R.A.L.vdH.)
†Current address: Department of Life Sciences, Imperial College, SW7 2AZ, London, UK
‡Current address: Leibniz Institute of Plant Biochemistry, Weinberg 3, 06120, Halle, Germany
§Current address: Department of Biomedicine, Aarhus University, Høegh-Guldbergsgade 10, DK-8000 Aarhus, Denmark
‖Current address: Laboratory of Plant Physiology, Plant Sciences Group, Wageningen University and Research, Droevendaalsesteeg 1, 6708PB, Wageningen, The Netherlands
¶Current address: Faculty of Biology, University of Freiburg, Schänzlestrasse 1, 79104 Freiburg, Germany
The author responsible for distribution of materials integral to the findings presented in this article in accordance with the policy described in the Instructions for Authors (https://academic.oup/com/plcell/pages/General-Instruction) is: Renier van der Hoorn (renier.vanderhoorn@biology.ox.ac.uk).

Abstract

Secreted immune proteases "Required for *Cladosporium* resistance-3" (Rcr3) and "*Phytophthora*-inhibited protease-1" (Pip1) of tomato (*Solanum lycopersicum*) are both inhibited by Avirulence-2 (Avr2) from the fungal plant pathogen *Cladosporium fulvum*. However, only Rcr3 acts as a decoy co-receptor that detects Avr2 in the presence of the Cf-2 immune receptor. Here, we identified crucial residues in tomato Rcr3 that are required for Cf-2-mediated signaling and bioengineered various proteases to trigger Avr2/Cf-2-dependent immunity. Despite substantial divergence in Rcr3 orthologs from eggplant (*Solanum melongena*) and tobacco (*Nicotiana* spp.), minimal alterations were sufficient to trigger Avr2/Cf-2-mediated immune signaling. By contrast, tomato Pip1 was bioengineered with 16 Rcr3-specific residues to initiate Avr2/Cf-2-triggered immune signaling. These residues cluster on one side of the protein next to the substrate-binding groove, indicating a potential Cf-2 interaction site. Our findings also revealed that Rcr3 and Pip1 have distinct substrate preferences determined by two variant residues and that both are suboptimal for binding Avr2. This study advances our understanding of Avr2 perception and opens avenues to bioengineer proteases to broaden pathogen recognition in other crops.

Introduction

The fungal pathogen *Cladosporium fulvum* (syn. *Passalora fulva*) causes leaf mold disease in cultivated tomato (*Solanum lycopersicum* L.). While most cloned resistance (*R*) genes of plants are nucleotide-binding oligomerization domain (NOD)-like receptors (NLRs), all cloned *R* genes against *C. fulvum* encode for cell surface-localized receptor-like proteins (RLPs) with extracellular leucine-rich repeats (LRRs). One such *R* gene encoding a LRR–RLP is *Cf-2*, which was introgressed into cultivated tomato from currant tomato (*Solanum pimpinellifolium*) (Dixon et al. 1996). *Cf-2* confers recognition of the secreted small cysteine-rich effector Avr2 of *C. fulvum* (Luderer et al. 2002), ultimately resulting in a localized programmed cell death called the hypersensitive response (HR) and stopping further pathogen growth.

Recognition of Avr2 by Cf-2 requires tomato *Rcr3*, which encodes a papain-like cysteine protease (PLCP; Krüger et al. 2002). PLCPs are stable, 20 to 25 kDa endopeptidases with a catalytic Cys–His–Asn triad that contains the catalytic Cys residue in a substrate-binding groove (Shindo and van der Hoorn 2008). PLCPs are produced as pre-pro-proteases that have a signal peptide for secretion and remain inactive until the autoinhibitory pro-domain is removed. The mature protease domain of Rcr3 is sufficient to trigger Avr2/Cf-2-dependent HR (Rooney et al. 2005), and Rcr3 activation in tomato is promoted by the highly abundant apoplastic subtilase P69B (Paulus et al. 2020).

Avr2 binds and inhibits mature Rcr3 and is not proteolytically processed by Rcr3 (Rooney et al. 2005). *Cf-2* tomato lines lacking *Rcr3* do not display obvious phenotypes (Dixon et al. 2000), and catalytically inactive Rcr3 can still bind Avr2 and trigger Cf-2-dependent HR (Paulus et al. 2020). These two facts indicate that it is not the substrate/product of Rcr3 that is recognized by Cf-2, but rather the Avr2/Rcr3 complex itself. Further studies using mutant Avr2 protein showed that the inhibition of Rcr3 by Avr2 corresponds with the induction of Cf-2-dependent HR (van't Klooster et al. 2011) and that Rcr3 homologs with the naturally occurring N194D substitution cannot be inhibited by Avr2 and do not trigger Avr2/Cf-2-dependent HR (Shabab et al. 2008; Hörger et al. 2012). Although these data all indicate that Cf-2

Received February 22, 2024. Accepted June 17, 2024

physically interacts with the Avr2/Rcr3 complex, this interaction remains to be demonstrated.

The indirect perception of Avr2 is consistent with the guard hypothesis, which proposes that immune receptors "guard" the virulence target of pathogen-derived effector proteins, rather than the effector itself (van der Biezen and Jones 1998; van der Hoorn et al. 2002; Dangl and Jones 2001). Accordingly, Cf-2 "guards" Rcr3 to monitor its manipulation by Avr2. Avr2 also inhibits Pip1 (*Phytophthora*-inhibited protease-1; Tian et al. 2007), a paralog of Rcr3 that is encoded by the same genomic locus but is evolving independently from Rcr3 in solanaceous plants (Ilyas et al. 2015; Kourelis et al. 2020). Pip1 is much more abundant than Rcr3, and Pip1 depletion by RNA interference increases susceptibility to *C. fulvum*, revealing that Pip1 is an immune protease and the operative virulence target for Avr2 (Ilyas et al. 2015). By contrast, in the absence of Cf-2, *rcr3* mutant lines are not more susceptible to *C. fulvum* infection, indicating that Rcr3 is not an operative target but acts as a decoy to trap the fungal pathogen into a recognition event in plants carrying Cf-2 (Shabab et al. 2008; van der Hoorn and Kamoun 2008).

Rcr3 and Pip1 evolved >50 million years ago (Mya) because homologs are present in solanaceous plants that diverged in this period (Kourelis et al. 2020). By contrast, Cf-2 only occurs in the *Solanum* genus which evolved ~8 Mya, indicating that Cf-2 co-opted an existing protease to detect its manipulation during infection (Kourelis et al. 2020). Most *Solanum* Rcr3 homologs can trigger Avr2/Cf-2-dependent HR, but many Rcr3 homologs outside the *Solanum* genus cannot, even though many can be inhibited by Avr2 (Kourelis et al. 2020). This indicates that the residues required for the interaction with Avr2, and those required for *Cf-2*-dependent Avr2 recognition are distinct, and is consistent with the adaptation of Cf-2 to guard Rcr3 in *Solanum* species.

Here, we investigated which residues in Rcr3 are required to trigger Avr2/Cf-2-dependent HR. This knowledge is required for future bioengineering of this perception system to mediate recognition of protease inhibitors produced by other plant pathogens and in other (crop) plants. To do this, we bioengineered three Rcr3-like proteases with increasing phylogenetic distance to *Solanum* Rcr3, starting with eggplant (*Solanum melongena*) Rcr3, then tobacco (*Nicotiana* spp.) Rcr3, and finally tomato Pip1. In all these proteases, we were able to bioengineer Avr2/Cf-2-dependent HR, providing intriguing insights into the evolution of this unique perception mechanism and an important platform for future decoy bioengineering.

Results

A single residue substitution in eggplant SmRcr3 is sufficient for Avr2/Cf-2-dependent HR

While tomato and potato Rcr3 homologs can complement Cf-2/Avr2-dependent HR in *Nicotiana benthamiana*, the eggplant (*S. melongena* L.) Rcr3 (*Sm*Rcr3) cannot trigger Cf-2/Avr2-dependent HR upon agroinfiltration (Kourelis et al. 2020). The mature protease domain of *Sm*Rcr3 differs at 45 residues from Rcr3 of *S. pimpinellifolium* (*Sp*Rcr3, here referred to as Rcr3, Fig. 1A). To identify a region in *Sm*Rcr3 that prevents signaling through Cf-2, we replaced three arbitrary, similar-sized parts of *Sm*Rcr3 with the corresponding Rcr3 sequence (Fig. 1B). *Sm*Rcr3 carrying part-4 of Rcr3 was able to confer Cf-2/Avr2-dependent HR, while *Sm*Rcr3 carrying part-5 of Rcr3 causes a very weak HR (Fig. 1C). Part-4 of *Sm*Rcr3 contains 12 variant residues, including one aspartic acid residue, (D244), which is a proline in all Rcr3 homologs that can trigger Cf-2/Avr2-dependent HR (Kourelis et al. 2020). Most other variant residues in part-4 are also different between *Solanum* Rcr3 homologs that can trigger Cf-2/Avr2-dependent HR.

*Sm*Rcr3 with the D244P mutation indeed triggers HR upon co-expression with Cf-2 and Avr2 (Fig. 1D). Furthermore, *Sm*Rcr3 produced upon agroinfiltration can be labeled with MV201 (Fig. 1E; Kourelis et al. 2020), a fluorescent activity-based probe for PLCPs (Richau et al. 2012), and preincubation with Avr2 prevents *Sm*Rcr3 labeling by MV201 (Fig. 1E). This confirms that *Sm*Rcr3 is an active protease that can be inhibited by Avr2. This inhibition is specific, as preincubation with Avr2 lacking the last six residues (Avr2Δ6), an inactive protease inhibitor (van't Klooster et al. 2011), does not prevent *Sm*Rcr3 labeling by MV201 (Fig. 1E). This experiment shows that a single D244P substitution is sufficient to bioengineer eggplant *Sm*Rcr3 into a protein that triggers Avr2/Cf-2-dependent HR and that interaction with Avr2 and with Cf-2 can be uncoupled in Rcr3 homologs.

We summarized the predicted location of the identified residues required for Avr2/Cf-2-dependent HR by creating structural models for *Sm*Rcr3 and the bioengineered *Sm*Rcr3(D224P) proteases using AlfaFold2 (Jumper et al. 2021). The structure of Avr2 could not be predicted by Alphafold2, probably because of a shallow multisequence alignment (MSA). By contrast, there is a robust MSA for the proteases. There are many well-resolved crystal structures for PLCPs, and the structures are predicted with a high predicted template modeling score (pTM = 0.94). As with all PLCPs, all protease models consist of two lobes with the substrate-binding groove in between. The catalytic Cys is located in the middle of that substrate-binding groove at the end of a long alpha helix and is in close proximity to the catalytic His and Asn residues. Residues in *Sm*Rcr3 that differ from Rcr3 scatter all over the front and back surfaces of these proteases (Fig. 1F, purple) although the substrate-binding groove is relatively similar. Most of these variant residues, however, are not required for Avr2/Cf-2-dependent HR. The D244P substitution locates at the edge of the substrate-binding groove and is predicted to have a minimal effect on the local structure of the protease (Fig. 1F), although the effect of missense mutations may be difficult to predict by AlphaFold2 (Buel and Walters 2022). Although *Sm*Rcr3(D244P) is not as active in triggering Avr2/Cf-2-dependent HR as tomato Rcr3, the fact that HR can be triggered with a single substitution in a protease that is so different from tomato Rcr3 is remarkable.

G194N substitution and a three-residue insertion in Nicotiana Rcr3 triggers Avr2/Cf-2-dependent HR

We previously found that *Nicotiana* Rcr3 homologs also cannot trigger Avr2/Cf-2-dependent HR (Kourelis et al. 2020). *Nicotiana* Rcr3 homologs differ at 49 residues and a 3-amino acid deletion in the protease domain compared to Rcr3 (Fig. 2A). While *N. benthamiana* lacks a functional Rcr3 homolog, we previously found that the inactivated *NbRcr3a* gene can be "resurrected" as an active protease, called r*Nb*Rcr3 (Kourelis et al. 2020). However, this r*Nb*Rcr3 cannot be inhibited by Avr2, probably because it lacks a key residue required for Avr2 inhibition (N194; Shabab et al. 2008; Hörger et al. 2012), which is a glycine in r*Nb*Rcr3.

To test whether the G194N substitution in r*Nb*Rcr3 promotes sensitivity for Avr2 inhibition, we preincubated r*Nb*Rcr3 and r*Nb*Rcr3(G194N) with Avr2, E-64, or Avr2Δ6 (van't Klooster et al. 2011) and labeled the remaining active protease with activity-based probe MV201. Detection by scanning the proteins upon separating on proteins gels for fluorescence showed that r*Nb*Rcr3

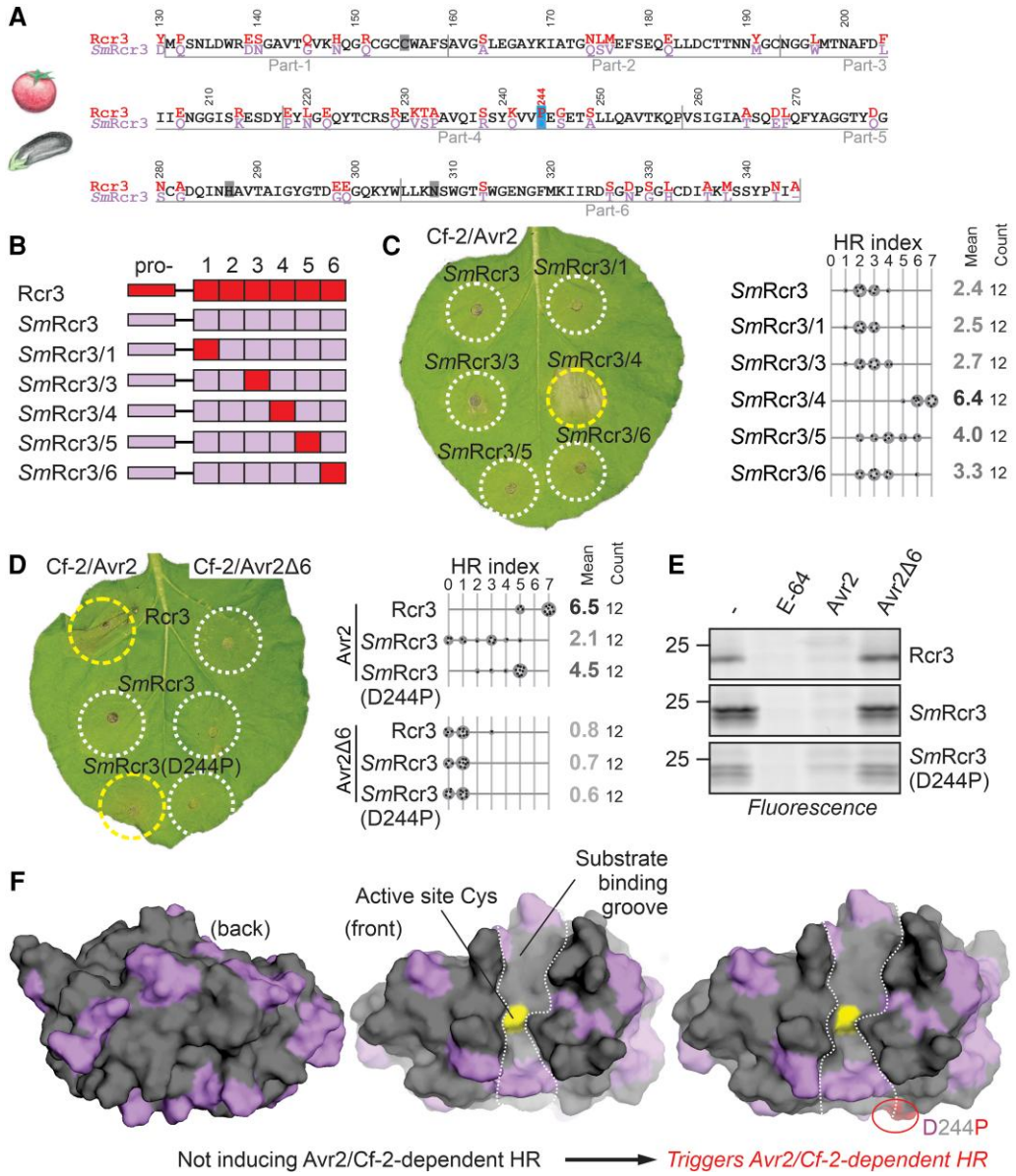

Figure 1. A single residue substitution in eggplant Rcr3 triggers Avr2/Cf-2-dependent HR. **A)** Alignment of tomato Rcr3 and *Sm*Rcr3 protein sequences. The numbering is based on the Rcr3 sequence of cultivated tomato (*Sl*Rcr3), which carries one additional amino acid in the prodomain compared to Rcr3. Residues are specific for Rcr3 (red) or *Sm*Rcr3 (violet) or occur in both (black). **B)** Tested Rcr3/*Sm*Rcr3 hybrids. The mature protease domain of *Sm*Rcr3 after the prodomain of *Sm*Rcr3 (pro-) was split into six parts, and each part was replaced by the corresponding part of Rcr3. **C)** *Sm*Rcr3 carrying part-4 of Rcr3 triggers Avr2/Cf2-2-dependent HR. *Sm*Rcr3 and five of its hybrids were transiently co-expressed with Avr2 and Cf-2 in *N. benthamiana*, and HR was scored 5 d later. Shown is a representative leaf with infiltrated regions encircled with a white line (no HR) or yellow line (HR). The HR index was determined using $n = 12$ replicates. Statistical analysis with the BestHR R package is provided in Supplementary File 3. **D)** *Sm*Rcr3 does not trigger Avr2/Cf2-2-dependent HR, but *Sm*Rcr3(D244P) does. Rcr3, *Sm*Rcr3, and *Sm*Rcr3(D244P) were transiently co-expressed with Avr2/Avr2Δ6 and Cf-2 in *N. benthamiana*, and HR was scored 5 d later. Shown is a representative leaf with infiltrated regions encircled with a white line (no HR) or yellow line (HR). The HR index was determined using $n = 12$ replicates. Statistical analysis with the BestHR R package is provided in Supplementary File 3. **E)** Rcr3, *Sm*Rcr3, and *Sm*Rcr3(D244P) are active proteases that can be inhibited by Avr2. AFs isolated from agroinfiltrated leaves transiently expressing Rcr3, *Sm*Rcr3, and *Sm*Rcr3(D244P) were preincubated for 45 min with and without 100 μM E-64, or 1 μM Avr2 or inactive Avr2Δ6 and then labeled for 3 h with 0.2 μM MV201. Samples were separated on SDS–PAGE gels and scanned for fluorescence. **F)** Structural models of *Sm*Rcr3 and bioengineered *Sm*Rcr3. Both sequences were modeled using AlphaFold2 (both pTM = 0.94) and presented in PyMol using surface representation of the front of the protease with residues that are identical to tomato Rcr3 (gray) and that are specific to *Sm*Rcr3 (purple). Bioengineering of *Sm*Rcr3 with D224P (red) causes Avr2/Cf-2-dependent HR.

carrying the G194N substitution can be inhibited by Avr2 (Fig. 2B). However, despite being Avr2-sensitive, co-expression with Avr2 and Cf-2 showed that r*Nb*Rcr3(G194N) does still not trigger Avr2/Cf-2-dependent HR (Fig. 2B and Supplementary Fig. S1).

All *Nicotiana* Rcr3 homologs lack three residues (D328/P329/S330) compared to Rcr3 homologs of *Solanum* and *Capsicum* (Kourelis et al. 2020). r*Nb*Rcr3 carrying G194N and these three additional residues [r*Nb*Rcr3(G194N + Asp-Pro-Ser {DPS})] is an active protease, is sensitive for Avr2 inhibition, and also triggers Avr2/Cf-2-dependent HR (Fig. 2B and Supplementary Fig. S1). By contrast, r*Nb*Rcr3(+DPS) is unable to interact with Avr2 and does not trigger Avr2/Cf-2-dependent HR (Fig. 2B and

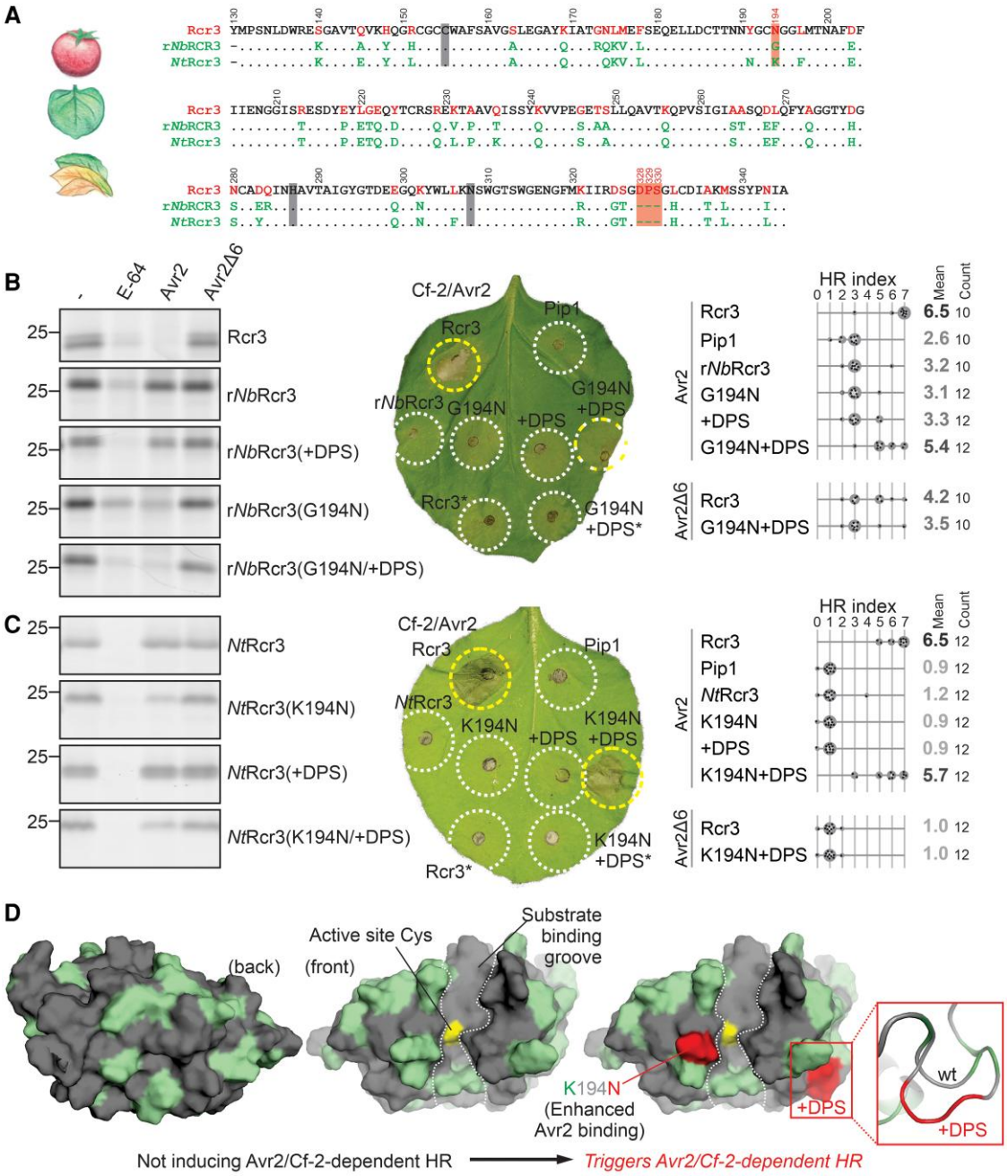

Figure 2. N194 and a three-residue insertion in *Nicotiana* Rcr3 trigger Avr2/Cf-2-dependent HR. **A)** Alignment of tomato Rcr3 with Rcr3 homologs from *N.benthamiana* (*Nb*) and *N. tabacum* (*Nt*). The numbering is based on the *Sl*Rcr3 sequence of cultivated tomato. Residues are specific for Rcr3 (red) or r*Nb*Rcr3/*Nt*Rcr3 (green) or occur in all (black). **B)** G194N substitution in resurrected *Nb*Rcr3 (r*Nb*Rcr3) reconstitutes Avr2 inhibition (left) and an additional three-residue insertion (+DPS) triggers Avr2/Cf-2-dependent HR (center and right panels). **C)** K194N substitution in tobacco *Nt*Rcr3 reconstitutes Avr2 inhibition (left) and an additional three-residue insertion (+DPS) triggers Avr2/Cf-2-dependent HR (center and right panels). **B), C)** Left gel images: AFs isolated from agroinfiltrated leaves transiently expressing (mutant) Rcr3 (homologs) were preincubated for 45 min with and without 100 μM E-64, or 1 μM Avr2 or inactive Avr2Δ6, and then labeled for 3 h with 0.2 μM fluorescent activity-based probe MV201 to detect the proteases that are not inhibited. Samples were separated on SDS–PAGE gels and scanned for fluorescence. Right HR assays: (mutant) Rcr3 homologs and Pip1 were transiently co-expressed with Avr2/Avr2Δ6 and Cf-2 in *N. benthamiana*, and HR was scored 5 d later. Shown is a representative leaf with infiltrated regions encircled with a white line (no HR), yellow line (HR), or both (intermediate HR). *, co-expressed with Avr2Δ6 instead of Avr2. The HR index was determined using $n = 12$ replicates. The gray scale of the average HR score (bold letters) correlates with the HR score. Statistical analysis with the BestHR R package is provided in Supplementary File 3. **D)** Structural models of *Nt*Rcr3 and bioengineered *Nt*Rcr3. Both sequences were modeled using AlphaFold2 (both pTM = 0.94) and presented in PyMol using surface representation of the front of the protease with residues that are identical to tomato Rcr3 (gray) and that are specific to *Nt*Rcr3 (green). Bioengineering of *Nt*Rcr3 with K194N and inserting tripeptide DPS (red) causes Avr2/Cf-2-dependent HR.

Supplementary Fig. S1). These data demonstrate that the DPS insertion is required for HR induction but not for Avr2 inhibition.

Like r*Nb*Rcr3, *N. tabacum* Rcr3 (*Nt*Rcr3) also lacks the DPS insertion and carries an N194 substitution, in this case into a lysine (K). As with r*Nb*Rcr3, Avr2 inhibition can be bioengineered into *Nt*Rcr3 with the K194N substitution, but these proteases do not trigger Avr2/Cf-2-dependent HR (Fig. 2C). The additional DPS insertion is also required to trigger Avr2/Cf-2-dependent HR (Fig. 2C).

*Nt*Rcr3 carrying only the DPS insertion is not inhibited by Avr2 and is unable to trigger HR (Fig. 2C). These data demonstrate again that the DPS insertion is required for HR induction in *Nicotiana* Rcr3 homologs but not for Avr2 inhibition.

Modeling the structure of both *Nt*Rcr3 and the engineered *Nt*Rcr3 with AlphaFold2 resulted in reliable models (pTM = 0.94), which shows that the variant residues in *Nt*Rcr3 when compared with tomato Rcr3 scatter over the surface on both sides of the protein (Fig. 2D, green residues). The K194N substitution is next to the catalytic Cys residue at the edge of the substrate-binding groove. This substitution promotes Avr2 binding, suggesting that Avr2 would interact with this residue and occupies the active site, consistent with its ability to suppress labeling with activity-based probe MV201, which labels the active site Cys residue. The insertion of the DPS tripeptide (D328/P329/S330) into *Nt*Rcr3 is predicted to extend a loop on the side of the protease (Fig. 2D). This DPS tripeptide locates in a similar region as the D224P mutation in *Sm*Rcr3, although in an adjacent loop. This indicates that the residues required for Avr2/Cf-2-dependent HR are clustered on the right lobe of the Rcr3 protease in both *Sm*Rcr3 and *Nt*Rcr3.

Pip1 triggers Avr2/Cf-2-dependent HR when carrying three parts of Rcr3

Next, we bioengineered *S. lycopersicum* Pip1 (*Sl*Pip1, here referred to as Pip1), a tomato immune protease that is even more distantly related to its paralog Rcr3 than *Sm*Rcr3 and *Nt*Rcr3 (Ilyas et al. 2015). The mature protease domains of Rcr3 and Pip1 differ at 93 residues, with several amino acid insertions and deletions (Fig. 3A). Pip1 can be inhibited by Avr2 (Shabab et al. 2008), but it does not trigger Avr2/Cf-2-dependent HR (Kourelis et al. 2020). One notable difference is that the DPS amino acid sequence in Rcr3, which is absent from *Nicotiana* Rcr3 and essential for Avr2/Cf-2-dependent HR, corresponds to a Val-Asp-Gly (VDG) sequence in Pip1 (Fig. 3A). Interestingly, this sequence is Val-His-Gly (VHG) in *S. pimpinellifolium* Pip1 (*Sp*Pip1) which has been co-introgressed with Rcr3 when creating the MM-Cf2 line. The D329H variant residue changing VDG into VHG is the only difference between mature Pip1 of cultivated tomato and *Sp*Pip1 of *S. pimpinellifolium*.

To identify the specific Rcr3 residues required for triggering Avr2/Cf-2-dependent HR, we divided Rcr3 into seven arbitrary similar-sized fragments and replaced corresponding segments in Pip1 with these Rcr3 fragments. As expected, the prodomain of Pip1 fused to the Rcr3 mature protease still triggers Avr2/Cf-2-dependent HR (Fig. 3B, construct 64), so all our remaining constructs carry the Pip1 prodomain. We next exchanged the six parts of the Pip1 protease domain with the corresponding parts of Rcr3. Out of the 64 possible combinations, we cloned and transiently expressed 57 Pip1/Rcr3 hybrids in *N. benthamiana* by agroinfiltration.

Of the 57 tested hybrid proteases, 33 were active proteases, as determined by MV201 labeling of apoplastic fluids (AFs) isolated from agroinfiltrated leaves (Fig. 3B and Supplementary Fig. S2). Given that all hybrids have an intact catalytic triad, we speculate that the 24 inactive Rcr3/Pip1 hybrids are unstable due to a disruption of the core structure of the protease caused by a mismatch of structural residues in the hybrids. Most unstable hybrids have either part-2 of Rcr3 combined with part-3 of Pip1, or part-3 of Pip1 combined with part-4 of Rcr3 (Fig. 3B). Of the 33 active proteases, 30 could be inhibited by Avr2 (Fig. 3B and Supplementary Fig. S3). The three Avr2-insensitive hybrid proteases contain combinations of residues H148, R151, E194, and Q284, which we previously showed to reduce Avr2 inhibition (Kourelis et al. 2020): construct 04 carries both E194 and Q284, whereas constructs 35 and 36 carry H148, R151, E194, and Q284. Interestingly, because Pip1 carries D148, V151, and R284 and Rcr3 carries only N194, this means that both Pip1 and Rcr3 are suboptimal interactors of Avr2.

Of the 30 Avr2-sensitive hybrid proteases, only eight can trigger *Cf-2*-dependent HR upon co-infiltration with Avr2 into leaflets of tomato MM-*Cf-2 rcr3-3* lines, which lack Rcr3 (Fig. 3B and Supplementary Fig. S3). All these HR-inducing hybrids are active proteases that can be inhibited by Avr2 (Fig. 3C). All the HR-inducing hybrids contain N194 in part-3, but many carry either D148 and V151 in part-1 or R284 in part-5, indicating that not all residues that strengthen the interaction with Avr2 are required for triggering HR. Pip1 carrying three parts from Rcr3 (parts 3, 5, and 6, see construct 12 in Fig. 3B) can trigger Avr2/Cf-2-dependent HR, which is consistent with the fact that all HR-inducing hybrids carry the same three Rcr3 parts (Fig. 3B). Replacing any of these Rcr3 parts for the corresponding Pip1 part results in a loss of HR (Fig. 3B), even though these proteases are active and inhibited by Avr2 (Supplementary Figs. S3 and S4). These data indicate that Avr2/Cf-2-dependent HR requires multiple residues residing in three of the six parts of the mature protease.

A more detailed, quantitative analysis of HR by co-expression of Pip1/Rcr3 hybrids with Avr2 and Cf-2 in *N. benthamiana* confirms that part-5 and part-6 of Rcr3 are required for inducing Avr2/Cf-2-independent HR, while part-3 makes an important contribution (Fig. 3D). Hybrid 12, containing part-3, part-5, and part-6 of Rcr3, can induce HR, whereas hybrids 10 and 11, lacking part-5 or part-6 from Rcr3, respectively, cannot induce HR (Fig. 3D). Hybrid 04, lacking part-3 of Rcr3, induces HR but to a quantitatively lesser extend (Fig. 3D). Notably, all these hybrids are active proteases that can be inhibited by Avr2 (Supplementary Fig. S2). Part-4 also contributes to the strength of HR, since constructs containing part-4 of Pip1 have a consistently reduced strength in inducing HR (Fig. 3D). However, this contribution to HR by part-4 of Rcr3 is relatively weak compared to part-3, part-5, and part-6, and part-4 was not investigated further.

Further mutagenesis identifies Rcr3 residues required for Avr2/Cf-2-dependent HR

To further identify critical residues in Rcr3 required to trigger Cf-2/Avr2-dependent HR, we took the Pip1 hybrid protease containing part-3, part-5, and part-6 from Rcr3 and made a series of substitutions in each Rcr3 part. These mutants were analyzed by activity-based protein profiling (ABPP) to confirm that they accumulate as active proteases, and co-expression with Avr2 and Cf-2 to determine the relative strength of HR induction.

Part-3 contains 10 variant residues and two deletions and includes the N194 residue which promotes Avr2 binding in Rcr3 when compared with E194 in Pip1 (Kourelis et al. 2020). We tested 11 mutants with various combinations of variant residues. Reflecting the quantitative contribution of part-3, all mutant proteases were able to trigger Avr2/Cf-2-dependent HR, albeit with varying strengths (Fig. 4A; Supplementary Data Set 1). Mutants carrying E194 from Pip1 were consistently less able to trigger HR when compared with those carrying N194 of Rcr3 (Fig. 4A), consistent with N194 promoting the interactions with Avr2 (Shabab et al. 2008; Hörger et al. 2012; Kourelis et al. 2020). No contributions to HR were identified for the other variant residues in part-3. These data indicate that N194 is the main contributor to HR in Rcr3 part-3.

Part-5 contains 19 variant residues and one deletion in Rcr3. Given the large number of variants, we focused on residues predicted to be solvent-exposed in AlphaFold2-generated models of

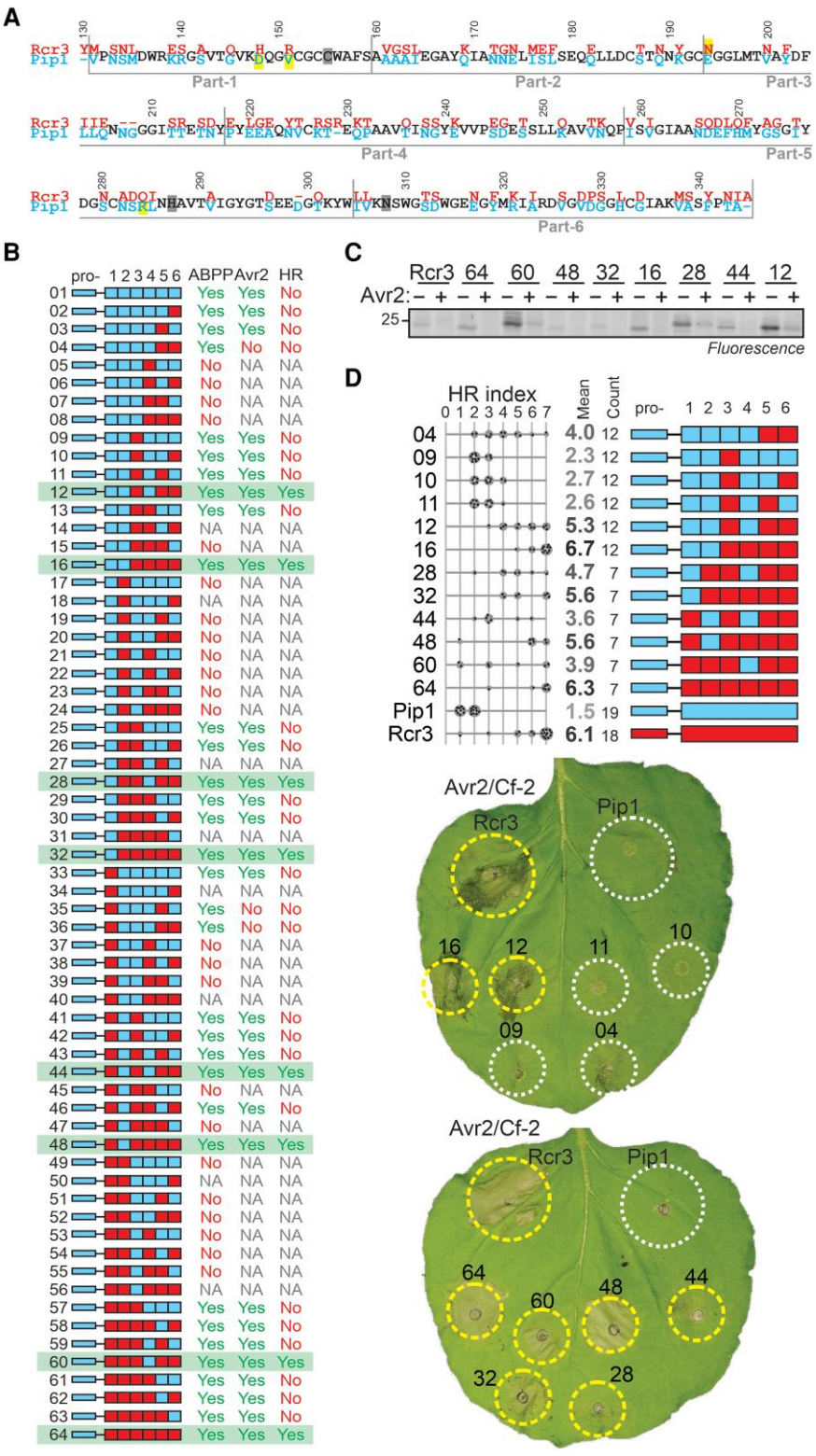

Figure 3. Pip1 triggers Avr2/Cf-2-dependent HR when carrying three parts of Rcr3. **A)** Amino acid alignment if Pip1 and Rcr3. The numbering is based on the SlRcr3 sequence of cultivated tomato. Four residues contributing to Avr2 inhibition are highlighted in yellow. **B)** Summary of analyzed Pip1/Rcr3 hybrids, showing construct number (pJK); domain architecture; labeling of the protease with MV201; inhibition by Avr2; and Avr2/Cf-2-dependent HR. NA, not analyzed. The eight Pip1/Rcr3 hybrids that trigger HR are highlighted in green. All constructs have the prodomain of Pip1 (pro-). **C)** Eight HR-inducing Pip1/Rcr3 hybrids are active proteases that can be inhibited by Avr2. AFs isolated from agroinfiltrated leaves transiently expressing Pip1/Rcr3 hybrids were preincubated for 45 min with and without 500 nM Avr2 and then labeled for 5 h with 0.2 μM MV201. Samples were separated on SDS–PAGE gels and scanned for fluorescence. **D)** Quantification of HR for selected Pip1/Rcr3 hybrids. Pip1/Rcr3 hybrids were transiently co-expressed with Avr2 and Cf-2 in *Nicotiana benthamiana*, and the HR was scored 5 d later. Shown is a representative leaf with infiltrated regions encircled with a white line (no HR) or yellow line (HR). The HR index was determined using $n = 12$ replicates. The gray scale of the average HR score (bold letters) correlates with the HR score. Statistical analysis with the BestHR R package is provided in Supplementary File 3.

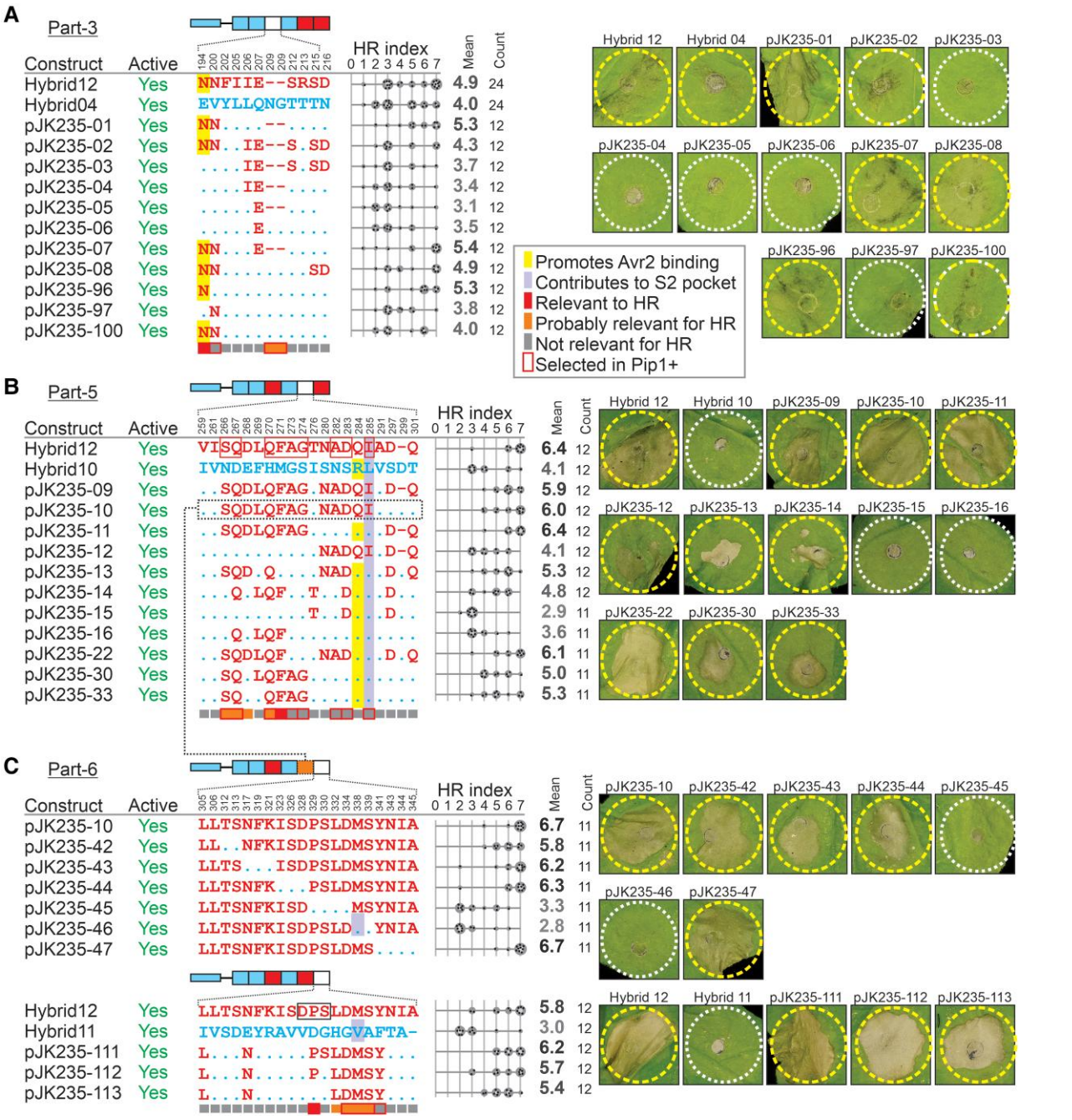

Figure 4. Further substitutions identify Rcr3 residues required for Avr2/Cf-2-dependent HR. Constructs tested to study variant residues in part-3 (**A**), part-5 (**B**), and part-6 (**C**) of the hybrid proteases. Shown on top is the general domain architecture of the listed constructs and below are the construct names; their activity detected by MV201 labeling; the variant residues in the respective parts with numbering of *Sl*Rcr3 on top; and the HR index upon co-expression with Avr2 and Cf-2 for $n = 12$ replicates. Residues of Rcr3 (red) or Pip1 (blue) important for binding Avr2 are highlighted yellow and residues required for triggering Cf-2/Avr2-dependent HR, or possibly contribution to triggering Cf-2/Avr2-dependent HR are flagged with red and orange blocks under the alignments, respectively. The gray scale of the average HR score (bold letters) correlates with the HR score. Statistical analysis with the BestHR R package is provided in Supplementary File 3.

the Rcr3/Pip1 protein structures. Construct pJK235-11, carrying only the 10 solvent-exposed Rcr3-specific residues and the amino acid deletion, still triggers a full HR (Fig. 4B; Supplementary Data Set 1), suggesting that the remaining nine residues are not involved in triggering HR. However, constructs pJK235-09 and 10, which include five additional Rcr3-specific residues (NADQI), caused reduced HR activity compared to pJK235-11 (Fig. 4B). This reduction correlates with the presence of Q284 from Rcr3, which is known to decrease Avr2 inhibition (Kourelis et al. 2020). Interestingly, constructs pJK235-09 and 10 display similar HR-inducing activity, indicating that the last three Rcr3-specific positions in part-5 (D-Q) do not significantly influence HR in the presence of Rcr3 residues NADQI. However, the comparison between constructs pJK235-11 and pJK235-30 suggests these residues (D-Q) do contribute quantitatively to HR (Fig. 4B). Similarly, the comparison between constructs pJK235-12, which contains NADQI and D-Q, and pJK235-30, which includes only the first stretch (SQDLQFAG), indicates that the first stretch alone has a more pronounced effect on HR induction, whereas the latter two stretches contribute to a lesser, yet discernible extent when combined.

Further analysis of constructs pJK235-14, pJK235-15, and pJK235-16 highlights the roles of individual residues. Construct pJK235-14, while weakly HR-active, differs significantly in HR induction from pJK235-15 and pJK235-16 (Fig. 4B), underscoring the importance of Q267 and/or the LQF sequence. The absence of either S266 or A273 and G274 requires either D283 or D297 for effective HR induction (Fig. 4B). Moreover, construct pJK235-22 triggers full HR (Fig. 4B), confirming that A273 and G274 are non-essential for HR. Its higher HR activity compared to pJK235-13 implies that L269 and F271 are contributors. Yet, the comparison of constructs pJK235-33 and pJK235-30 reveals that L269 does not contribute significantly, indicating a role for F271 in HR induction in pJK235-22. In summary, while most of the 19 variant positions in part-5 do not contribute significantly to HR, residues S266, Q267, D268, Q270, and F271 (SQD-QF) collectively contribute to HR. Additionally, Pip1 residue R284 contributes to HR quantitatively by enhancing Avr2 inhibition, along with quantitative contributions to HR by N280/A282/D283 and D297/Q302.

Finally, part-6 contains 19 variant residues and one insert/deletion amino acid. Part-6 also contains the DPS insertion required for *Nicotiana* Rcr3 s to trigger Avr2/Cf-2-dependent HR (Fig. 2), but this sequence is VDG in Pip1. To further pinpoint residues in part-6, we first tested the effect of replacing six regions with Pip1 residues in pJK235-10, which also carries seven Pip1-specific residues in part-5. This scan revealed that Rcr3-specific residues TS, NFK, ISD, and YNIA are not essential for HR and that Rcr3-specific residues PSLD and MS contain residues that are essential for triggering HR (Fig. 4C; Supplementary Data Set 1). Thus, the D328 in the DPS motif is not required for triggering HR. Constructs pJK235-111 and 112 have similar HR-inducing activity (Fig. 4C), indicating that S330 in the DPS motif is also not required. pJK235-113, however, is less able to trigger HR (Fig. 4C), which indicates that P329 in the DPS motif is important for HR. In conclusion, P329 and the combination of four variant residues (LDMS) are the only four Rcr3-specific residues contributing to HR in part-6.

Pip1+ differs by only 18 residues from Rcr3 and triggers Avr2/Cf-2-dependent HR

While we were still analyzing the role of the variant residues within part-3, part-5, and part-6, we generated Pip1+, which is a Pip1 protease that contains only 18 Rcr3-specific residues (Fig. 5A), including 11 of the 13 variant residues that were associated with HR. The two missing residues are D268 and L332, which were not tested separately but were found to contribute to HR in conjunction with other variant residues. The selection of these 18 residues involved systematically removing Rcr3-specific residues from part-3, part-5, and part-6 through a three-step process: firstly, by omitting residues with <50% exposure in Rcr3 structural models; secondly, by excluding variants present in natural Rcr3 orthologs from *Solanum* species; and thirdly, by removing chemically similar variants in Pip1 orthologs (Supplementary Fig. S5). Pip1+ therefore contains N194 (enhances Avr2 binding); N200; the two-residue deletion in part-3 (ΔNG); S266; Q267; Q270; F271; A273; G274; A282; D283; I285; P329; D334; M338; S339; and Y341. Pip1+ still has 78 (84%) of the variant residues in the protease domain and shares 94.8% identity with Pip1 across the entire protein and only 53.8% with Rcr3. Importantly, the co-expression of Pip1+ with Avr2 and Cf-2 triggers HR with similar strength as Rcr3 (Fig. 5B), confirming that most of the variant residues do not contribute to HR.

Modeling the structure of both Pip1 and the engineered Pip1+ with AlphaFold2 resulted in reliable models (pTM = 0.94), which shows that the variant residues in Pip1 when compared with tomato Rcr3 scatter over the surface on both sides of the protein (Fig. 5C, red residues). Most of these variant residues, however, are not required for Avr2/Cf-2-dependent HR. Pip1 carries VDG instead of the DPS insertion missing from *Nt*Rcr3, but a D329P substitution in this extended loop is essential to induce Avr2/Cf-2-dependent HR. It seems likely that the P329 proline residue will restrict the folding flexibility of the VDG loop but such structural change was not predicted using Alphafold2 modeling. Pip1 requires N194 to enhance Avr2 binding and trigger Avr2/Cf-2-dependent HR, similar to *Nt*Rcr3. The remaining residues required for Avr2/Cf-2-dependent HR in Pip1 all cluster on the top of the β-sheet lobe (Fig. 5C), which represents a likely platform for interactions with Cf-2.

Pip1 and Rcr3 have distinct substrate specificities

To investigate whether Rcr3 and Pip1 may have distinct substrate specificities, we used a modified version of proteomic identification of protease cleavage sites (PICS) with an *Escherichia coli* proteome-derived peptide library generated by digestion with trypsin and Lys-C (Biniossek et al. 2016) (Fig. 6A). With this library, we assessed substrate specificity of recombinant Pip1, Rcr3, and *Sl*Rcr3, which were produced in *Pichia pastoris* and purified via a C-terminal His tag (Paulus et al. 2020). As with other papain-like Cys proteases, Rcr3 and Pip1 also display selectivity for a hydrophobic P2 residue in the substrate (Fig. 6B), but the selectivity is distinctly different. Both Rcr3 and *Sl*Rcr3 share a preference for P2 being either proline (P), methionine (M), valine (V), or leucine (L) (Fig. 6B). By contrast, Pip1 prefers P2 being either leucine (L) or phenylalanine (F) (Fig. 6B). This indicates that Rcr3 and Pip1 have distinct substrate specificities and therefore likely have distinct substrates.

We next analyzed the structural models of Rcr3 and Pip1 to investigate the underlying reason for their differing substrate specificity. Variant residues I285L and M338 V constitute the edge of the S2 pocket, opposite to the catalytic Cys (Fig. 6C). The I285 and M338 residues in Rcr3 seem to keep the S2 pocket small, explaining the accommodation of smaller Val and Pro residues at the P2 position in substrates. By contrast, the L285 and V338 residues in Pip1 seem to extend the S2 pocket, explaining the accommodation of the much larger Phe(F) residues at the P2 position of the substrate. Thus, the putative larger S2 pocket in Pip1 might be why it can accommodate substrates with P2 = Phe, in contrast to Rcr3, which prefers smaller residues at P2.

Dipeptide substrates show that Pip1+ has an Rcr3 substrate preference

To confirm the difference in substrate specificity of Rcr3 and Pip1, we took advantage of two commercially available dipeptide substrates, z-FR-AMC and z-LR-AMC, which release fluorescent 7-amido-4-methylcoumarin (AMC) upon cleavage. According to PICS data, Rcr3 should preferentially cleave z-LR-AMC, whereas Pip1 should prefer z-FR-AMC. We transiently expressed Pip1 and Rcr3 by agroinfiltration and purified them using C-terminal His tags (Schuster et al. 2022). Catalytic mutants of each of these proteases were included as negative controls. Incubation of Rcr3 and Pip1 with these two substrates indeed confirmed their distinct substrate specificity: Rcr3 preferentially cleaves z-LR-AMC and Pip1 preferentially cleaves z-FR-AMC (Fig. 6D).

To test whether Pip1+ has maintained the substrate specificity of Pip1, we produced Pip1+ and its catalytic mutant by agroinfiltration and purified it using a C-terminal His tag. Remarkably,

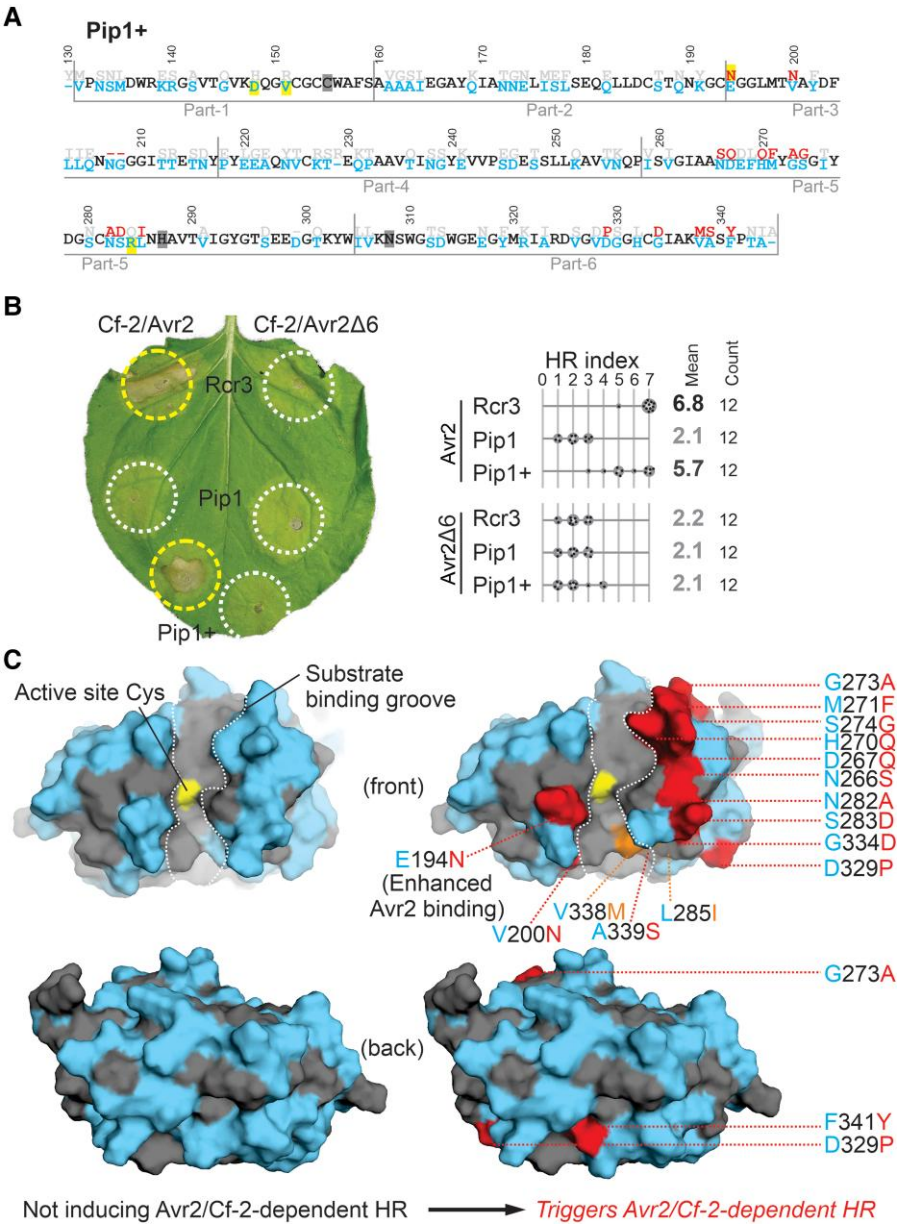

Figure 5. Pip1+ contains only 18 Rcr3-specific positions and triggers Avr2/Cf-2-dependent HR. **A)** Protein sequence of the protease domain of Pip1+, showing residues specific to Rcr3 (red), Pip1 (blue), or both (black). The four residues promoting Avr2 affinity are highlighted in yellow and the active site residues in gray. **B)** Pip1+ triggers Avr2/Cf-2-dependent HR. Rcr3, Pip1, and Pip1+ were transiently co-expressed with Cf-2 and Avr2/Avr2Δ6 in *N. benthamiana* by agroinfiltration. Shown is a representative leaf with infiltrated regions encircled with a white line (no HR) or yellow line (HR). The HR index was determined using $n = 12$ replicates. The gray scale of the average HR score (bold letters) correlates with the HR score. Statistical analysis with the BestHR R package is provided in Supplementary File 3. **C)** Structural models of Pip1 and bioengineered Pip1+ . Both sequences were modeled using AlphaFold2 (both pTM = 0.94) and presented in PyMol using surface representation of the front of the protease with residues that are identical to tomato Rcr3 (gray) and that are specific to Pip1 (light blue). Bioengineering of Pip1 with 16 Rcr3-specific residues (red/orange) causes Avr2/Cf-2-dependent HR. Two Rcr3-specific substitutions (V338 M and L285I, orange) alter substrate specificity.

enzymatic assays showed that Pip1+ preferentially cleaves z-LR-AMC, unlike Pip1 and similar to Rcr3 (Fig. 6E). Thus, by introducing Rcr3-specific residues into Pip1, we also changed the substrate specificity of Pip1.

S2 pocket bioengineering reverts the substrate specificity of Pip1++

To test whether the modified S2 pockets in Pip1+ are responsible for Rcr3-like substrate specificity, we generated Pip1++, which contains the L285 and V338 of Pip1 and is otherwise identical to Pip1+, carrying 16 Rcr3-specific residues. Enzymatic assays using purified proteases showed that Pip1++ exhibits significantly increased activity toward z-FR-AMC when compared to Pip1+, consistent with the enlarged S2 pocket while retaining a high activity for z-LR-AMC (Fig. 6D). This indicates that the S2 pocket can be bioengineered to revert the altered substrate specificity toward that of Pip1.

To determine whether Pip1++ is also able to trigger HR with Avr2 and Cf-2, we co-expressed Pip1++ with Avr2 and Cf-2 by agroinfiltration and monitored the strength of HR. Pip1++ triggers a strong HR with Avr2 but not with Avr2Δ6, similar to Rcr3 (Fig. 6E). Thus, although bioengineering the S2 pocket in Pip1+ changed its substrate specificity, it did not diminish its ability to trigger HR with Avr2 and Cf-2.

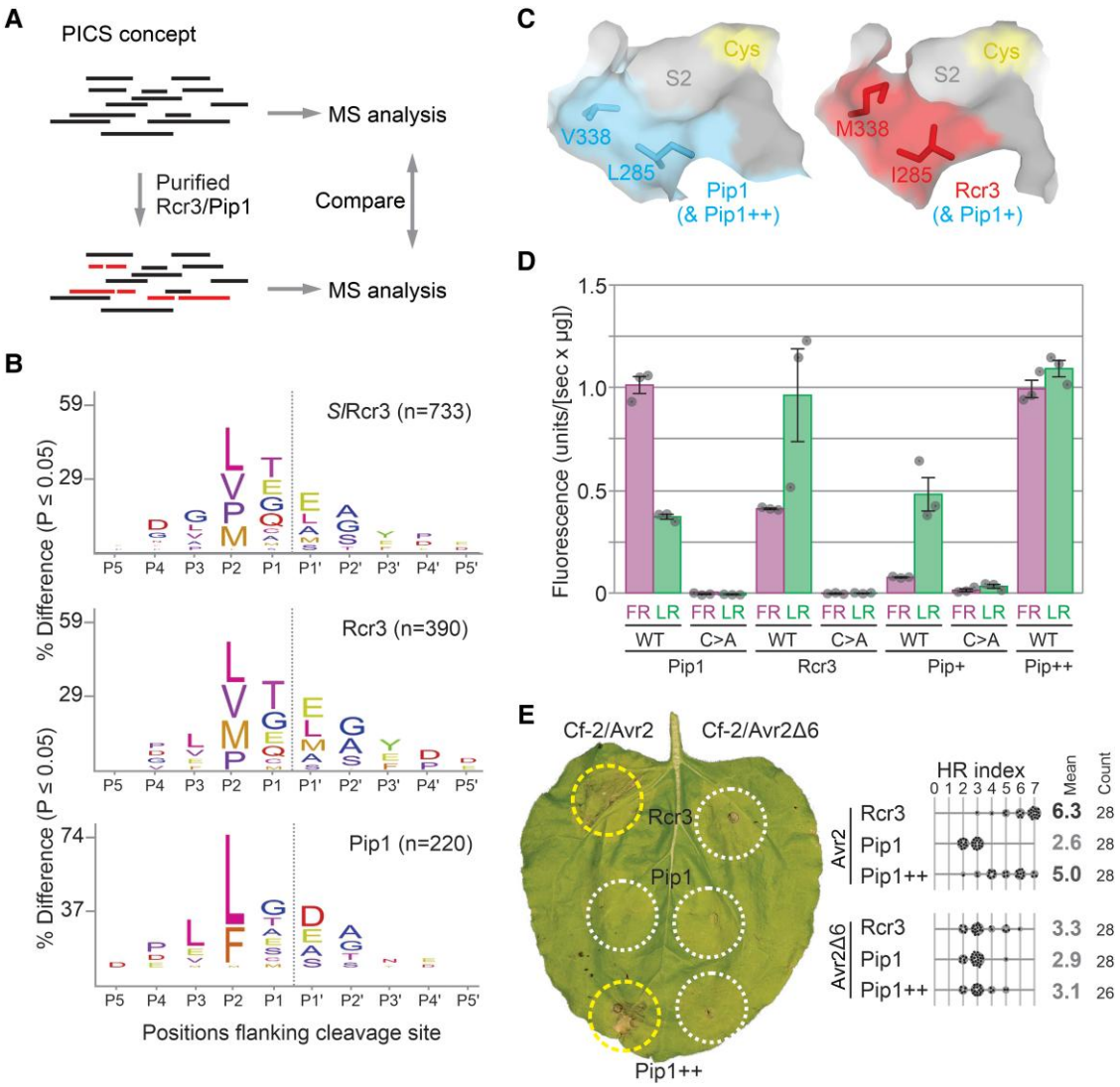

Figure 6. S2 pocket bioengineering reverts substrate specificity of Pip1+. **A**) Determination of cleavage site preference using proteomic identification of protease cleavage sites (PICS). A trypsin digest of *E. coli* is incubated with and without various proteases, isotopically labeled by reductive demethylation, mixed with the buffer control, and analyzed by tandem MS. Differences with the internal buffer control (red) are used to select cleaved peptides and generate the cleavage logo. **B)** Cleavage logos for *Sl*Rcr3, Rcr3 (*Sp*Rcr3), and Pip1. A peptide library made using trypsin/LysC from an *E. coli* proteome was digested with recombinant C-terminal 6xHis-tagged Rcr3 and Pip1 purified from *P. pastoris*. This digested peptide library was di-methylated, mixed in equal amounts, and analyzed by LC–MS/MS. A custom PERL script was used to filter semi-specific peptides and through database-lookup determine the corresponding prime and nonprime sequence. Shown are the residues relative to the cleavable bond, and their frequencies are used to scale the font size. The number of all and unique cleavage events that was used to calculate the cleavage logo is indicated. **C)** Model for the different S2 pockets in Rcr3 and Pip1. Structural models were generated for Rcr3 and Pip1 with Alphafold2, and the S2 substrate-binding pocket was visualized in PyMol with 50% surface presentation. Shown are the catalytic Cys (yellow) and the variant residues in Rcr3 (red) and Pip1 (blue). **D)** Different dipeptide preferences for Pip1, Rcr3, Pip1+, and Pip1++. Pip1, Rcr3, Pip1+, and Pip1++ and their catalytic mutants were produced by agroinfiltration and purified via their C-terminal His tag. Equal protein amounts were incubated with zLR-AMC and zFR-AMC, and fluorescence was read using a plate reader for $n = 3$ replicates. The fluorescence intensity measured over 60 min was plotted for all samples. This experiment was repeated with independently produced proteases with similar results. **E)** Pip1++ triggers Avr2/Cf-2-dependent HR. Rcr3, Pip1, and Pip1++ were transiently co-expressed with Cf-2 and Avr2/Avr2Δ6 in *N. benthamiana* by agroinfiltration. Shown is a representative leaf with infiltrated regions encircled with a white line (no HR) or yellow line (HR). The HR index was determined using $n = 28$ replicates. The gray scale of the average HR score (bold letters) correlates with the HR score. Statistical analysis with the BestHR R package is provided in Supplementary File 3.

Discussion

We found that bioengineering eggplant Rcr3 with a single D244P substitution is sufficient to trigger Avr2/Cf-2-dependent HR. This residue does not affect the interaction with Avr2 and is likely to affect interaction with Cf-2. We also discovered that the insertion of three residues (D328/P329/S330) into *N. tabacum* Rcr3 or the resurrected *N. benthamiana* Rcr3, together with the G194N or K194N substitutions, is sufficient for Avr2/Cf-2-dependent HR. While the G194N and K194N substitutions are required for increased Avr2 binding, the D328/P329/S330 insertion is only required for HR and is absent from all *Nicotiana* Rcr3 homologs. In addition, a series of Rcr3/Pip1 hybrids revealed three regions in Rcr3 important for Avr2/Cf-2-dependent HR. Further fine-mapping uncovered that the HR-relevant residues cluster on one lobe of Rcr3, flanking the substrate-binding groove. Substitutions at the rim of the S2 pocket altered substrate specificity in Pip1+, but these substitutions are not essential for HR and reconstitute Pip1-like activity when mutated to Pip1-like residues in Pip1++.

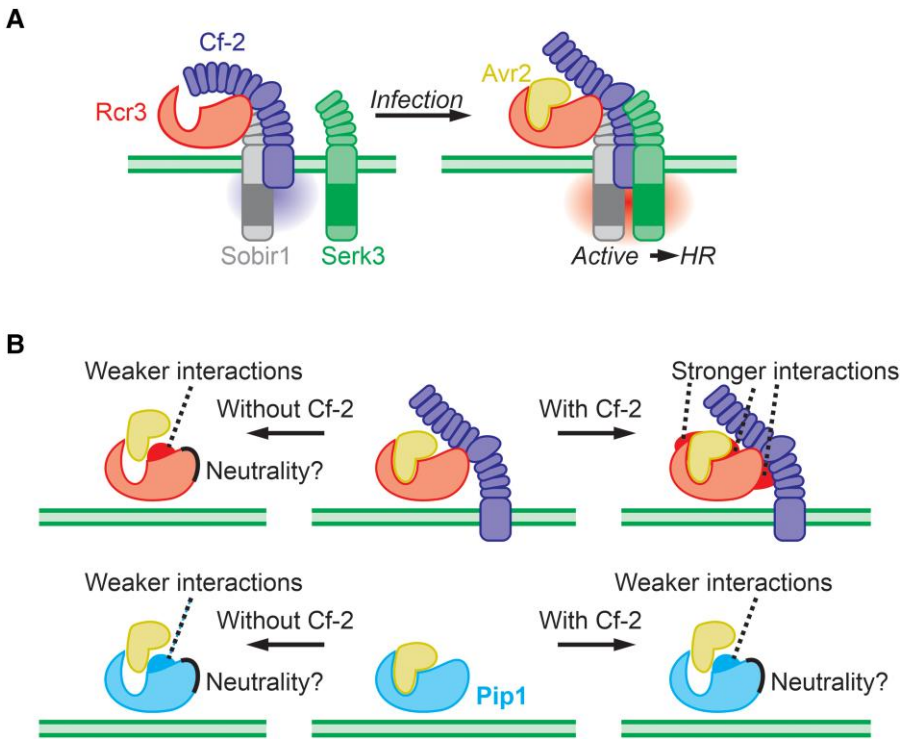

Figure 7. Working model of Avr2 perception and Rcr3 evolution. **A)** In noninfected plants, Rcr3, Cf-2, and Sobir1 are interacting in a constitutive complex lacking SERK3. Upon infection, Avr2 would bind Rcr3 with high affinity, triggering a conformational change in Cf-2 that triggers the recruitment of SERK3, which then activates the HR. **B)** Rcr3 is under opposing selection pressures in the presence/absence of Cf-2, at the putative interfaces with both Avr2 and Cf-2. By contrast, Pip1 will be under selection to avoid Avr2 inhibition and will probably not be under selection to interact with Cf-2.

Our findings lead us to propose a working model in which the Avr2/Rcr3 complex interacts with Cf-2 (Fig. 7A). In the Pip1++ mutant, the residues essential for Avr2/Cf-2-dependent HR are predominantly located on the top of the β-sheet lobe next to the substrate-binding groove. This specific localization suggests that Cf-2 likely binds this region, enabling it to simultaneously detect the presence of Avr2 bound to the substrate-binding pocket of Rcr3. We hypothesize that the binding of the Avr2/Rcr3 complex induces a conformational change in Cf-2, triggering HR. This process likely involves recruiting somatic embryogenesis receptor kinase-3 (SERK3 also known as BRI1-accociated kinase-1), as observed in other RLPs, including Cf-4 (Postma et al. 2016). This activated immune complex would lead to the activation of NRC3, thereby inducing HR and immunity toward the pathogen (Kourelis et al. 2022).

The presence of Rcr3 and Pip1 in solanaceous plants while Cf-2 is specific to the *Solanum* genus (Kourelis et al. 2020) indicates that Rcr3 is under diverse selection pressures in different plant species. In *Solanum* plants that have Cf-2, selection pressure will be on increasing Avr2/Rcr3 and Rcr3/Cf-2 interactions, while in the absence of Cf-2 in *Solanum* plants, the selection pressure will be on Rcr3 to avoid inhibition by Avr2 (Fig. 7B). This should cause opposing selection forces in two distinct areas of Rcr3: residues required for Cf-2-dependent HR will be under selection to increase interactions with Cf-2 only in *Solanum* and evolve under neutrality in other solanaceous plants. This could explain why eggplant and tobacco Rcr3 carry D244 and the DPS deletion, respectively, which both abolish HR signaling with Cf-2. Further evolutionary studies of Rcr3 in wild solanaceous plants may elucidate the ancestral state of Rcr3 and may show how Rcr3 is adapted in *Solanum* to mediate Cf-2-dependent HR signaling. The second area under selection in Rcr3 includes the residues around the substrate-binding groove where inhibitors bind: the "ring-of-fire" (Hörger and van der Hoorn 2013). These "ring-of-fire" positions are indeed highly variant (Shabab et al. 2008) and under diversifying selection in Rcr3 (Hörger et al. 2012). Indeed, four of these variant residues affect Avr2 affinity (Kourelis et al. 2020). These and other variant residues might also affect interactions with other Rcr3 inhibitors such as Cip1 and EpiCs (Song et al. 2009; Shindo et al. 2016; Schuster et al. 2024). Further studies of Rcr3 in wild solanaceous plants could reveal the different selection pressures on these residues, depending on the presence of Cf-2 and the inhibitors used by different pathogens. Although the selection pressure on Pip1 is much less than on Rcr3, variant residues also accumulated around the substrate-binding groove (Shabab et al. 2008), consistent with arms races with various pathogen-derived inhibitors. Modification of two of these residues (D147R and V150E) renders Pip1 insensitive to Pip1 inhibitor EpiC2B (Schuster et al. 2024). Residues that are required for Cf-2-mediated HR in Rcr3 might be under neutrality or negative selection in Pip1, although it is interesting that the only variant residue between Pip1 and *Sp*Pip1 (H329D) is at one such position. Further studies on the occurrence of variant residues in Rcr3 and Pip1 and their relevance to disease and immunity may uncover strengths and directionalities of selection on these immune proteases.

Our attempts to physically demonstrate interactions of Avr2/Rcr3 or Rcr3 with Cf-2, including co-immunoprecipitation assays and blue native gel electrophoresis, have been unsuccessful so far, despite the availability of active Avr2 and Rcr3 proteins (e.g. Paulus et al. 2020), and a good expression of the soluble ectodomain of Cf-2 in *N. benthamiana*. This suggests that additional specific conditions or cofactors might be required to recapitulate the Avr2/Rcr3/Cf-2 complex in in vitro assays. Although the interactions between some pathogen-secreted effector proteins and proteases such as the tomato-secreted P69B protease can be successfully predicted with AlphaFold Multimer (AFM; Homma et al. 2023), we were

unsuccessful in similarly predicting the structure of the Avr2/Rcr3/Cf-2 complex. The inability of AFM to predict a reliable structure of Avr2 is probably caused by the low number of available Avr2-homologous sequences, while the large LRR region of Cf-2 can easily support false-negative complexes predicted by AFM. Interactions between Cf-2 and Avr2/Rcr3 are likely but remain to be demonstrated.

*Sl*cr3 of cultivated tomato (SlRcr3) is able to trigger Cf-2-dependent auto-necrosis in tomato (Krüger et al. 2002), but this can be suppressed in hybrids that co-express the *Sp*Rcr3 allele, which co-evolved with Cf-2 in *S. pimpinellifolium* (Ilyas et al. 2015). This indicates that SlRcr3 has a lower affinity for Cf-2 and can be outcompeted by Rcr3. The ability of SlRcr3 to trigger auto-necrosis with Cf-2 is only detected in tomato and could not be established in *N. benthamiana* (Kourelis et al. 2020), which might suggest that tomato expresses a co-factor that binds SlRcr3 more strongly than Rcr3 and triggers HR in a similar way as Avr2 does. Rcr3 has also been reported to trigger Cf-2-dependent HR with potato cyst nematode (*Globodera rostochiensis*) effector *Gr*VAP1 (Lozano-Torres et al. 2012), but we were unable to reproduce these results (Kourelis et al. 2020). By contrast, both the *Pseudomonas syringae* pv. *tomato* DC3000 chagasin-like effector Cip1 and the *Phytophthora infestans* cystatin-like effectors EpiC1 and EpiC2B can inhibit Rcr3, but they do not trigger *Cf*-2-dependent HR (Shindo et al. 2016; Song et al. 2009). One reason for not triggering Cf-2-dependent HR might be that Cf-2 may not be able to directly interact with the effector in the Cip1/Rcr3 and EpiC/Rcr3 complexes. A second reason might be that both Cip1 and EpiCs are relatively weak inhibitors of Rcr3, as they both preferentially inhibit immune protease C14 (Kaschani et al. 2010; Shindo et al. 2016). Avr2 has a much higher affinity for Rcr3 (Kaschani et al. 2010; Shindo et al. 2016) and might be able to insert itself into a preformed Rcr3/Cf-2 complex, causing a conformational change in Cf-2 that triggers HR. The latter model would be consistent with the presence of an endogenous inhibitor of tomato that binds stronger to SlRcr3 than to Rcr3, explaining the auto-necrosis induced by SlRcr3 but not Rcr3. This model indicates that bioengineered Rcr3 with increased affinity to Cip1 and/or EpiCs could confer Cf-2-dependent immunity to *Pseudomonas syringae* and/or *Phytophthora infestans*, respectively. Although the Rcr3/Pip1 hybrids generated in this study were not able to induce Cf-2-dependent HR in the presence of either Cip1 or EpiCs (Supplementary Fig. S4), we did not yet generate and test Rcr3 variants with an increased affinity to these effectors.

A similar concept of "decoy bioengineering" has previously been demonstrated for pseudokinase PBS1, which is a decoy in the recognition of AvrPphB, a type-III protease effector produced by *Pseudomonas syringae*, by resistance protein RPS5, a NLR in *Arabidopsis thaliana* (Kim et al. 2016). PBS1 contains a cleavage site for AvrPphB, and replacing this cleavage site with that of other pathogen-produced proteases triggered RPS5 activation by proteases of these other pathogens, resulting in immunity to *P. syringae* expressing the AvrRpt2 protease effector or to turnip mosaic virus expressing its viral protease (Kim et al. 2016; Pottinger et al. 2020). Interestingly, in other plant species, PBS1 homologs are similarly guarded by unknown NLRs through a process of convergent evolution (Carter et al. 2019). Bioengineering these PBS1 homologs in soybean or potato can also provide immunity against different viral pathogens, even without knowing the identity of the NLR guarding these PBS1 homologs (Helm et al. 2019; Pottinger et al. 2020; Bai et al. 2022). This suggests that it is possible that decoy bioengineering could provide an alternative route to an altered recognition spectrum.

Indeed, some NLRs are able to interact with different decoys in nature. One notable example is the highly conserved NLR ZAR1 (Adachi et al. 2023; Gong et al. 2022), which interacts with different (pseudo)kinases to recognize different effectors (Lewis et al. 2013; Wang et al. 2015; Seto et al. 2017; Schultink et al. 2019; Laflamme et al. 2020; Martel et al. 2020). In the case of ZAR1, the (pseudo)kinases appear to be under evolutionary pressure to diversify (Gong et al. 2022). Similarly, Rcr3 is under selection to diversify at residues surrounding the substrate-binding groove (Hörger et al. 2012), possibly to create alleles that confer recognition of other pathogen-secreted protease inhibitors. Decoy bioengineering may provide an alternative route for the generation of synthetic resistance genes targeting important plant pathogens in the future. Finally, it is important to note that Cf-2 is not the only cell surface receptor that has been shown to require additional apoplastic factors for ligand recognition, as the apoplastic protein auxin-binding protein-1 (ABP1) and ABP1-LIKE 1 and 2 physically interact with the LRR–RLP transmembrane kinase family receptor-like kinases to form an auxin-sensing complex in the apoplast (Yu et al. 2023).

Our enhanced understanding of Rcr3 can now be applied to exploit the Rcr3/Cf-2 perception system to provide immunity to different pathogens through decoy bioengineering. PLCPs, such as Pip1 and Rcr3, are universally secreted by plants, including in key crops such as maize, citrus, rice, and papaya where they play a vital role in defending the apoplast against pathogen colonization (Misas-Villamil et al. 2016). In response, many host-adapted apoplastic pathogens secrete PLCP inhibitors to facilitate colonization, as seen in pathogens such as the maize smut pathogen *Ustilago maydis* (Mueller et al. 2013), the citrus Huanglongbing pathogen *Candidatus Liberibacter asiaticus* (Clark et al. 2018), the crucifer clubroot pathogen *Plasmodiophora brassicae* (Pérez-López et al. 2021), the tomato bacterial spot pathogen *Pseudomonas syringae* (Shindo et al. 2016), and the potato late blight pathogen *Phytophthora infestans* (Tian et al. 2007). Bioengineering the Rcr3/Cf-2 perception system to recognize these PLCP inhibitors can be an effective and sustainable approach to develop a perception system that confers recognition of the many different bacterial, fungal, and oomycete pathogens that secrete PLCP inhibitors when colonizing the apoplast.

Materials and methods

Plant material and growth conditions

Wild-type and mutant *N. benthamiana* and *S. lycopersicum* MoneyMaker (MM)-*Cf-2 rcr3-3* (Dixon et al. 2000) were propagated in a glasshouse and, for most experiments, grown in a controlled growth chamber with temperature maintained at 22 to 25°C, humidity at 45% to 65%, and a 16-/8 -h light/dark cycle. Lighting was provided by a combination of two Philips Master TL-D 58W/840 and Sylvania GRO-LUX F58W/GRO-T8 fluorescent tubes.

General plasmid constructions

The Golden Gate Modular Cloning (MoClo) kit (Weber et al. 2011) and the MoClo plant parts kit (Engler et al. 2014) were used for cloning, and all vectors are from this kit unless specified otherwise. Unless stated otherwise, receptors, effectors, and Rcr3 variants were cloned into the binary vector pJK268c, which contains the tomato bushy stunt virus silencing inhibitor p19 in the backbone (Paulus et al. 2020). Cloning design and sequence analysis were done using Geneious Prime (v2022.2.1; https://www.geneious.com). Plasmid construction including sequences of

used primers and synthetic DNA fragments is described in Supplementary Data Set 2.

Fragment-swapped hybrid cloning

For fragment-swapping the nucleotide region encoding for the Rcr3 and Pip1, peptidase C1 domain was divided into six arbitrary fragments and ordered through gene-synthesis (Biomatik; pJK103 to pJK107, pJK111 to pJK115, pJK185, pJK186; Supplementary Data Set 2). These fragments, together with a fragment containing the nucleotides encoding for the Pip1 prodomain but lacking the signal peptide (pJK110; Supplementary Data Set 2), were combined in all 64 possible combinations with pICH41264 (Addgene #4799; Weber et al. 2011) in a BpiI Golden Gate reaction (Supplementary Data Set 2). These fragment-swapped level 0 modules were subsequently combined with pJK001 and pJK002 (Grosse-Holz et al. 2018) and pICH51288 and pICH41414 (2×35S and 35S terminator; Addgene #50269 and #50337; Engler et al. 2014) in a BsaI Golden Gate reaction to generate binary vectors containing the fragment-swapped Rcr3/Pip1 hybrids driven by the double 35S CaMV promoter and targeted to the apoplast using a *Nt*PR1a signal peptide. All used and created plasmids are summarized in Supplementary Data Set 2.

E. coli expression vector cloning Avr2, Cip1, EpiC1, and EpiC2B purification

The expression vectors for periplasmic secretion of N-terminal 6xHis-tagged Avr2 (pJK153; pET28b-ProT7:OmpA-6xHis-TEV-Avr2) or Avr2Δ6 (pSM101; pET28b-ProT7:OmpA-HIS-TEV-Avr2Δ6) (Kourelis et al. 2020), and Cip1 (pJK159; pET28b-ProT7:OmpA-6xHis-TEV-Cip1), or C-terminal 6xHis-tagged EpiC1 (pJK254; pET28b-ProT7:OmpA-EPIC1-6xHis) and EpiC2B (pJK256; pET28b-ProT7:OmpA-EPIC2B-6xHis), were generated as described in Supplementary Data Set 2 and transformed into *E. coli* strain Rosetta2(DE3)pLysS (Novagen/Merck).

For protein purification, an overnight grown starter culture was diluted 1/100 in Terrific Broth [(per liter: 24 g yeast extract, 12 g bacto-tryptone, 0.5% v/v glycerol), after autoclaving, 0.2 M/L potassium phosphate buffer (26.8 g KH_2PO_4 and 173.2 g K_2HPO_4, pH 7.6) was added], and the bacteria were grown for ∼3 h to $OD_{600} \approx 0.6$ and induced overnight at 37 °C upon adding 0.8 mM isopropyl β-D-1-thiogalactopyranoside. The supernatant was collected by centrifuging the bacterial culture at 10,000×*g* at 4 °C for 20 min, adjusted to 50 mM Tris–HCl, 150 mM NaCl, and 10 mM imidazole, and run over a Ni-NTA agarose (Qiagen)-loaded column by gravity flow. The Ni-NTA agarose was washed with 10 column volumes (CV) washing buffer (50 mM Tris–HCl, 150 mM NaCl, 50 mM imidazole, pH 8), and the protein was eluted using elution buffer (50 mM Tris–HCl, 150 mM NaCl, 250 mM imidazole, pH 8). The purified protein was concentrated by centrifugation in 3 kDa cut-off filters (Amicon Ultra-15 Centrifugal Filter Units, Merck) at 4,500×*g* at 4 °C, flash-frozen in liquid nitrogen, and stored at −80 °C. Protein concentration was determined by Bradford assay using BSA as a standard, and purity was verified by running the protein on 18% w/v SDS–PAGE gels followed by Coomassie staining.

Transient gene expression and cell death assays

Transient gene expression in *N. benthamiana* was performed by agroinfiltration according to the methods described by van der Hoorn et al. (2000). Briefly, *A. tumefaciens* strain GV3101 pMP90 cells carrying binary vectors were inoculated from glycerol stock in LB supplemented with appropriate antibiotics and grown overnight at 28 °C until saturation. Cells were harvested by centrifugation at 2,000×*g* at room temperature for 5 min and resuspended in infiltration buffer (10 mM $MgCl_2$, 10 mM MES–KOH, pH 5.6, 200 μM acetosyringone) to OD_{600} 0.25 for each construct in the stated combinations and left to incubate in the dark for 2 h at room temperature prior to infiltration into young, fully expanded leaves of 5-wk-old *N. benthamiana* plants. Replicate numbers given indicate independent infiltration of different leaves from multiple plants. For quantitation, HR cell death phenotypes were scored in a range from 0 (no visible necrosis) to 7 (fully confluent necrosis) as in Kourelis et al. (2022) and plotted using a R script modified from Bentham et al. (2023). Statistical analysis was conducted using the besthr R package (MacLean 2020).

Experimental design and replicates

Up to eight leaf spots were infiltrated per leaf, up to three leaves per plant were used, and a minimum of three plants per combination were included in the experiments. HR quantification was done on a single experiment; constructs were independently tested, but HR was not quantified in other cases.

HR assays in tomato

AF was isolated from agroinfiltrated *N. benthamiana* plants expressing different Rcr3/Pip1 protein variants at 5 d post-infiltration. Briefly, the AF was extracted by vacuum infiltrating *N. benthamiana* leaves with ice-cold MilliQ. Leaves were dried with filter paper to remove excess liquid, and AF was extracted by centrifugation of the leaves in a 20-ml syringe barrel (without needle or plunger) located in a 50 ml falcon tube at 2,000×*g* at 4 °C for 25 min. 1 μM Avr2 (final concentration) was added to this AF, which was infiltrated into leaflets of tomato MM-*Cf-2 rcr3-3* plants (Dixon et al. 2000). Leaves were imaged 2 to 5 dpi.

Activity-based protein-profiling

AF was isolated from agroinfiltrated *N. benthamiana* plants expressing different proteins at 2 to 3 d post-infiltration, and samples were used directly in labeling reactions. Samples were adjusted to 5 mM DTT, 50 mM NaAc, pH 5.0, and preincubated for 45 min with either 100 μM E-64 (a general PLCP inhibitor), 2 μM purified Avr2 or Avr2Δ6, or 1% v/v DMSO (final concentration) as a control. After preincubation, samples were labeled with 2 μM MV201 for 3 h at room temperature (total volume 50 μl) (Richau et al. 2012). The labeling reaction was stopped by precipitation with five volumes of ice-cold acetone, followed by a 10-s vortex and immediate centrifugation at 16,100×*g* at 4 °C for 5 min. Samples were resuspended in a 2× sample buffer (100 mM Tris–HCl, pH 6.8), 200 mM DTT, 4% w/v SDS, 0.02% w/v bromophenol blue, 20% v/v glycerol) and boiled at 95 °C for 5 min prior to separation on 15% v/v SDS–PAGE gels. Fluorescence scanning was performed on an Amersham Typhoon-5 scanner (GE Healthcare) using Cy3 settings. Equal loading was verified by Coomassie staining (Pink et al. 2010).

P. pastoris expression vector cloning and protein purification

The *P. pastoris* PichiaPink yeast expression system was used to produce C-terminally 6xHis-tagged *Sl*Rcr3 (pPINKα-HC-*Sl*Rcr3-6xHis), Rcr3 (pJK206; pPINKα-HC-Rcr3-6xHis), and Rcr3(C153A/C154A) (pJK209; pPINKα-HC-Rcr3(C153A/C154A)-6xHis) (Paulus et al. 2020), or Pip1 (pJK211; pPINKα-HC-Pip1-6xHis) (Supplementary

Data Set 2). The proteases were cloned after the dibasic KR Kex2 protease cleavage site of the N-terminal secretion signal from the *S. cerevisiae* α-factor and driven by the methanol-induced *AOX1* promoter.

10 μg of plasmid DNA linearized using SpeI was transformed into electrocompetent PichiaPin strain 4 (ThermoFisher; *P. pastoris* genotype *ade2*, *pep4*, *prb1*) targeted to the *TRP2* locus, followed by selection on PAD selection plates (ThermoFisher) and selection of white colonies indicative of multiple integrations. Glycerol stocks were prepared by concentrating the transformants to a final OD_{600} of 50 to 100 (~2.5 to 5.0 × 10^9 cells/ml) in 25% v/v glycerol, and aliquots were snap-frozen in liquid nitrogen and stored at −80 °C.

For protein expression, a single glycerol stock was thawed and used to inoculate a 25-ml starter culture of Buffered Glycerol Complex Medium (BMGY) medium [1% w/v yeast extract; 2% w/v peptone; 100 mM potassium phosphate, pH 6.0; 1.34% w/v yeast nitrogen base (YNB) with ammonium sulfate and without amino acids; 0.00004% w/v biotin; 1% v/v glycerol] in a 250-ml baffled flask, grown at 30 °C at 300 rpm until the culture reached an OD_{600} of 2 to 6 (~2 to 3 d). This starter culture was used to inoculate 1 l of BMGY divided over four 1-l baffled flasks and grown at 30 °C at 300 rpm until the culture reached log-phase growth (OD_{600} = 2 to 6). Cells were harvested by centrifugation in sterile centrifuge bottles at 3,000×g for 5 min at room temperature. To induce expression, the supernatant was decanted, and the pellet was resuspended in 200 ml of BMMY medium (1% w/v yeast extract; 2% w/v peptone; 100 mM potassium phosphate, pH 6.0; 1.34% w/v YNB with ammonium sulfate and without amino acids; 0.00004% w/v biotin; 0.5% v/v methanol). This culture was divided between two 1-l baffled flasks which were covered with two layers of sterile gauze, and grown for 24 h at 30 °C at 300 rpm. Afterward, the supernatant was collected by centrifugation of the culture at 10,000×g at 4 °C for 20 min. The supernatant was adjusted to 150 mM NaCl and 30 mM imidazole and run over a Ni-NTA agarose (Qiagen)-loaded column by gravity flow. The Ni-NTA agarose was washed with 10 CV of washing buffer (50 mM Tris–HCl, 150 mM NaCl, 50 mM imidazole, pH 8), and the protein was eluted using elution buffer (50 mM Tris–HCl, 150 mM NaCl, 250 mM imidazole, pH 8). Finally, the purified protein was concentrated by centrifugation in 3 kDa cut-off filters (Amicon Ultra-15 Centrifugal Filter Units, Merck) at 4,500×g at 4 °C, flash-frozen in liquid nitrogen, and stored at −80 °C. Protein concentration was determined by Bradford assay using BSA as a standard, and purity was verified by running the protein on 15% v/v SDS–PAGE gels followed by Coomassie staining.

Proteomics identification of cleavage sites (PICS) peptide library preparation

Proteome-derived peptide libraries were produced essentially as described (Demir et al 2022). Briefly, proteins were extracted from an *E. coli* cell pellet in 6 M guanidine–HCl,100 mM HEPES, 150 mM NaCl, adjusted to pH 7.5 and supplemented with 10 mM EDTA and 1 mM phenylmethylsulfonyl fluoride (PMSF) directly before use. Proteins were reduced with 10 mM DTT and alkylated with 40 mM iodoacetamide at 25 °C, the reaction quenched after 60 min with another 10 mM DTT. Proteins were purified by chloroform/MeOH precipitation, resuspended in 100 mM HEPES, pH 7.5, and digested at 37 °C overnight with trypsin/Lys-C (Promega) at a protease-to-proteome ratio of 1:100 (wt/wt). A small aliquot was analyzed by SDS–PAGE to assure complete digestion. Digestion proteases were inhibited with 1 mM PMSF and heating to 70 °C for 20 min, and the sample was acidified with 0.5% v/v trifluoroacetic acid and degassed by application of a mild vacuum. Peptides were purified on Sep-Pak C18 solid-phase extraction cartridges (Waters) according to the manufacture's protocol, and the resulting peptide library was stored in aliquots at a peptide concentration of 2 mg/ml at −80 °C.

PICS specificity assay

100 μg of the PICS peptide library was used per treatment. The peptide library was diluted to 1 mg/ml (final concentration) in 50 mM NaAc, pH 5, and 10 mM Tris(2-carboxyethyl)phosphine (TCEP; final concentration). Purified proteases (Rcr3-His, SlRcr3-His, or Pip1-His) or control (buffer) was matured in 50 mM NaAc pH 5 and 10 mM TCEP (final concentration) for 5 h, prior to addition at a ratio of 1:100 (wt/wt), and incubated for 1 h at room temperature. 100 μM E-64 (final concentration) was added to inactivate the proteases, and proteases were further heat-inactivated for 5 min at 95 °C. Protease-treated and control samples were isotopically labeled by reductive dimethylation. Rcr3-, SlRcr3-, Pip1-, and buffer-treated samples were labeled with either 20 mM $^{12}CH_2O$ (cat. no. 252549, Sigma-Aldrich) and 20 mM $NaBH_3CN$ (cat. no. 252549, Sigma-Aldrich) (light), 20 mM $^{12}CD_2O$ (Sigma-Aldrich) and 20 mM $NaBH_3CN$ (medium), or 20 mM $^{13}CD_2O$ (cat. no. 596388, Sigma-Aldrich) and 20 mM $NaBD_3CN$ (Sigma-Aldrich) (heavy), respectively, and incubated overnight at 37 °C. Afterward, an additional 20 mM formaldehyde (final concentration 40 mM) and 20 mM sodium cyanoborohydride (40 mM final concentration) were added to ensure complete labeling. Labeling was quenched by the addition of 100 mM Tris–HCl, pH 6.8, and 60-min incubation at 37 °C. Following labeling, protease-treated and control samples were mixed at equal ratios and desalted by C18 solid-phase extraction (Sep-Pak, Waters) according to the manufacturer's instructions and concentrated to 10 μl using a vacuum concentrator (ThermoFisher).

MS data acquisition and analysis

For MS analysis of the PICS samples, 3 μl of the desalted samples were loaded onto a C18 reverse-phase capillary trap column (Acclaim PepMap C18, 75 μm × 2 cm, 3 μm particle size, Thermo) and separated using a C18 reverse-phase analytical column (Acclaim PepMap C18, 75 μm × 25 cm, 2 μm particle size, 100 Å, Thermo) coupled to an UltiMate3000 nano RSLC system (Thermo). A 90-min gradient from 5% to 32% v/v acetonitrile 0.1% v/v formic acid in H_2O was used to elute the peptides at a flow rate of 300 nl min^{-1}. The nano-LC system was on-line coupled to an Impact II high-resolution quadrupole-time-of-flight tandem mass spectrometer (Bruker) using a CaptiveSpray nano-electrospray source (Beck et al. 2015). MS spectra were acquired in a range from m/z 200 to 1,750 at 4 Hz. For fragmentation, the 17 most intense precursor ions of each MS scan were selected (Top 17 method). MS/MS spectra of the fragmented precursor ions were recorded in a mass range from m/z 300 to 1,750 at an intensity-dependent collection rate of 2 to 20 Hz spectrum. The sample was injected twice.

Peptides were identified and quantified using the MaxQuant software package, version 1.6.0.16 (Tyanova et al. 2016). Generic settings for Bruker Q-TOF instruments were used to match spectra to protein sequences to the *E. coli* proteome database (strain K12, reference proteome, 4,308 entries). Search parameters included precursor mass tolerance of ±10 ppm, fragment ion mass tolerance of ±20 ppm, semi-tryptic peptides with up to one missed cleavage, cysteine carboxyamidomethylation (+57.02 Da), lysine, and N-terminal dimethylation (light formaldehyde 28.0313 Da;

medium formaldehyde 32.0564 Da; heavy formaldehyde 36.0756 Da) as static modifications, and methionine oxidation and deamidation of asparagine and glutamine as variable modifications. A false discovery rate of 0.01 was applied for both spectrum-to-sequence matching and protein identification. A custom PERL script was used to filter semi-specific peptides and through database-lookup determine the corresponding prime and non-prime sequence (Demir et al 2022). Sequence logos showing substrate specificity were calculated as iceLogos using a local installation (Colaert et al. 2009).

In-planta protein production and purification

C-terminally tagged Pip1 (pJK083; pL2M-P19-Pro2x35S:Pip1-6xHis), Pip1(C153A/C154A) (pJK083; pL2M-P19-Pro2x35S:Pip1(C153A/C154A)-6xHis), Rcr3 (pJK026; pL2M-P19-Pro2x35S:Rcr3-6xHis), Rcr3(C153A/C154A) (pJK145; pL2M-P19-Pro2x35S:Rcr3(C153A/C154A)-6xHis), Pip1+ (pJK674; pL2M-P19-Pro2x35S:Pip1+-6xHis), Pip1+ (C153A/C154A) (pJK675; pL2M-P19-Pro2x35S:Pip1+ (C153A/C154A)-6xHis), and Pip1++ (pJK676; pL2M-P19-Pro2x35S:Pip1++-6xHis) were produced and purified from *N. benthamiana* as previously described (Schuster et al. 2022). Briefly, proteins were transiently produced by agroinfiltration as described above. Six days post-infiltration AF was extracted as described above. Protein purification was performed at 4 °C to prevent protease self-degradation. 250 μL Ni-NTA resin (Qiagen) was equilibrated with 20 CV ice-cold purification buffer (50 mM Tris–HCl, pH 7.4, 150 mM NaCl) in a small gravity column (Mini Bio-Spin, BioRad). 8 to 10 ml AF containing the His-tagged proteins was loaded twice onto the resin. The Ni-NTA agarose was washed with 10 CV washing buffer (50 mM Tris–HCl, 150 mM NaCl, 10 mM imidazole, pH 8), and the protein was eluted using elution buffer (50 mM Tris–HCl, 150 mM NaCl, 50 mM imidazole, pH 8). Finally, the purified protein was concentrated by centrifugation in 3 kDa cut-off filters (Amicon Ultra-15 Centrifugal Filter Units, Merck) at 4,500×g at 4 °C, flash-frozen in liquid nitrogen, and stored at −80 °C. Protein purity was verified by running the protein on 15% v/v SDS–PAGE gels followed by Coomassie staining.

Substrate specificity assay

1 μg of pure protein was incubated in reaction buffer (50 mM sodium acetate, pH 5.0, 10 mM DTT) supplemented with either 4 mM FR-AMC (Sigma) or LR-AMC (Bachem) substrate. Fluorescence was measured using a 96-well plate reader (Tecan Infinite M200) every 20 s for 2 h at ex360/em460, and the 1-h timepoint was selected for data visualization. Data points were analyzed based on detected total changes in emission, relative to t0.

Accession numbers

SmRcr3: Smechr0201177; NbRcr3: Nbe.v1.s00060g37460; NtRcr3: XP_009775922.1 with V61 M and K318R and V337L; Rcr3pim: AAM19207.1; Pip1: ABG23376.1; Cf-2: AAC15780.1

Acknowledgements

The authors thank Urszula Pyzio for excellent plant care; Sarah Rodgers, Caroline O-Brian and Patricia Bowman for technical assistance; John Baker for photography; and Sylvestre Marillonnet and Nicola Patron for providing plasmids via AddGene.

Author contributions

J.K. generated most of the dataset by cloning, protease expression, ABPP, and HR analysis; M.S. purified immune proteases and performed assays with fluorescent dipeptides; F.D. and P.F.H. performed PICS analysis on purified proteases provided by J.K.; O.M., S.K., P.S.K., R.O., S.R., A.L.B.C., and B.C.M. supported the analysis of the mutant proteases by transient expression and/or ABPP and/or HR assays; J.K., S.K., and R.A.L.vdH. conceived the project; and J.K. and R.A.L.vdH. wrote the article with input from all co-authors.

Supplementary data

The following materials are available in the online version of this article.

Supplementary Figure S1 *Nb*Rcr3(G184N + DPS) induces Avr2/Cf-2-dependent HR.

Supplementary Figure S2 Thirty-three Pip1/Rcr3 hybrids are active proteases.

Supplementary Figure S3 Thirty Pip1/Rcr3 hybrids can be inhibited by Avr2.

Supplementary Figure S4 Eight Pip1/Rcr3 hybrids trigger Avr2/Cf-2-dependent HR.

Supplementary Figure S5 Selection of Rcr3-specific residues that may contribute to HR.

Supplementary Data Set 1. HR data for Rcr3 variants.

Supplementary Data Set 2. Plasmid construction.

Supplementary File 1: Uncropped gels.

Supplementary File 2: Plasmid maps.

Supplementary File 3: Scripts, raw data, and statistics for HR quantification.

Funding

This work was supported by "The Clarendon Fund" (J.K.) and the European Research Council ERC-CoG-2013 grant 616449 "GreenProteases" (R.H., J.K.); European Reseaerch Council ERC-AdG-2020 grant 101019324 "ExtraImmune" (B.M. and R.H.); and BBSRC 18RM1 grant BB/S003193/1 "Pip1S" (M.S. and R.H.). The funders had no role in study design, data collection and analysis, decision to publish, or preparation of the manuscript.

Conflict of interest statement: None declared, except for J.K., whom received funding from industry during part of this study.

Data availability

Uncropped gels are provided in Supplementary File 1. Used plasmids are listed in Supplementary Data Set 2, and plasmid maps are provided in Supplementary File 2.

References

Adachi H, Sakai T, Kourelis J, Pai H, Gonzalez Hernandez JL, Utsumi Y, Seki M, Maqbool A, Kamoun S. Jurassic NLR: conserved and dynamic evolutionary features of the atypically ancient immune receptor ZAR1. *Plant Cell*. 2023:35(10):3662–3685. https://doi.org/10.1093/plcell/koad175

Bai R, Li H, Du W, Niu N, Li W, Gao Q, Yao C, Zhou Z, Bao W, Che M, et al. Decoy engineering of the receptor-like cytoplasmic kinase StPBS1 to defend against virus infection in potato. *Mol Plant Pathol*. 2022:23(6):901–908. https://doi.org/10.1111/mpp.13220

Beck S, Michalski A, Raether O, Lubeck M, Kaspar S, Goedecke N, Baessmann C, Hornburg D, Meier F, Paron I, et al. The impact II,

a very high-resolution quadrupole time-of-flight instrument (QTOF) for deep shotgun proteomics. *Mol Cell Proteomics*. 2015:14(7):2014–2029. https://doi.org/10.1074/mcp.M114.047407

Bentham AR, De la Concepcion JC, Benjumea JV, Kourelis J, Jones S, Mendel M, Stubbs J, Stevenson CEM, Maidment JHR, Youles M, et al. Allelic compatibility in plant immune receptors facilitates engineering of new effector recognition specificities. *Plant Cell*. 2023:35(10):3809–3827. https://doi.org/10.1093/plcell/koad204

Biniossek ML, Niemer M, Maksimchuk K, Mayer B, Fuchs J, Huesgen PF, McCafferty DG, Turk B, Fritz G, Mayer J, et al. Identification of protease specificity by combining proteome-derived peptide libraries and quantitative proteomics. *Mol Cell Proteomics*. 2016:15(7):2515–2524. https://doi.org/10.1074/mcp.O115.056671

Buel GR, Walters KJ. Can AlphaFold2 predict the impact of missense mutations on structure? *Nat Struct Mol Biol*. 2022:29(1):1–2. https://doi.org/10.1038/s41594-021-00714-2

Carter ME, Helm M, Chapman AVE, Wan E, Restrepo Sierra AM, Innes RW, Bogdanove AJ, Wise RP. Convergent evolution of effector protease recognition by *Arabidopsis* and barley. *Mol Plant Microbe Interact*. 2019:32(5):550–565. https://doi.org/10.1094/MPMI-07-18-0202-FI

Clark K, Franco JY, Schwizer S, Pang Z, Hawara E, Liebrand TWH, Pagliaccia D, Zeng L, Gurung FB, Wang P, et al. An effector from the Huanglongbing-associated pathogen targets citrus proteases. *Nat Commun*. 2018:9(1):1718. https://doi.org/10.1038/s41467-018-04140-9

Colaert N, Helsens K, Martens L, Vandekerckhove J, Gevaert K. Improved visualization of protein consensus sequences by iceLogo. *Nat Methods*. 2009:6(11):786–787. https://doi.org/10.1038/nmeth1109-786

Dangl JL, Jones JDG. Plant pathogens and integrated defence responses to infection. *Nature*. 2001:411(6839):826–833. https://doi.org/10.1038/35081161

Demir F, Kuppusamy M, Perrar A, Huesgen PF. Profiling sequence specificity of proteolytic activities using proteome-derived peptide libraries. *Meth Mol Biol*. 2022:2447:159–174. https://doi.org/10.1007/978-1-0716-2079-3_13

Dixon MS, Golstein C, Thomas CM, van der Biezen EA, Jones JDG. Genetic complexity of pathogen perception by plants: the example of *Rcr3*, a tomato gene required specifically by *Cf-2*. *Proc Natl Acad Sci U S A*. 2000:97(16):8807–8814. https://doi.org/10.1073/pnas.97.16.8807

Dixon MS, Jones DA, Keddie JS, Thomas CM, Harrison K, Jones JDG. The tomato *Cf-2* disease resistance locus comprises two functional genes encoding leucine-rich repeat proteins. *Cell*. 1996:84(3):451–459. https://doi.org/10.1016/S0092-8674(00)81290-8

Engler C, Youles M, Gruetzner R, Ehnert T-M, Werner S, Jones JDG, Patron NJ, Marillonnet S. A Golden Gate modular cloning toolbox for plants. *ACS Synth Biol*. 2014:3(11):839–843. https://doi.org/10.1021/sb4001504

Gong Z, Qi J, Hu M, Bi G, Zhou J-M, Han G-Z. The origin and evolution of a plant resistosome. *Plant Cell*. 2022:34(5):1600–1620. https://doi.org/10.1093/plcell/koac053

Grosse-Holz F, Madeira L, Zahid MA, Songer M, Kourelis J, Fesenko M, Ninck S, Kaschani F, Kaiser M, van der Hoorn RAL. Three unrelated protease inhibitors enhance accumulation of pharmaceutical recombinant proteins in *Nicotiana benthamiana*. *Plant Biotechn J*. 2018:16(10):1797–1810. https://doi.org/10.1111/pbi.12916

Helm M, Qi M, Sarkar S, Yu H, Whitham SA, Innes RW. Engineering a decoy substrate in soybean to enable recognition of the soybean mosaic virus NIa protease. *Mol Plant Microbe Interact*. 2019:32(6):760–769. https://doi.org/10.1094/MPMI-12-18-0324-R

Homma F, Huang J, van der Hoorn RAL. AlphaFold-Multimer predicts cross-kingdom interactions at the plant-pathogen interface. *Nat Commun*. 2023:14(1):6040. https://doi.org/10.1038/s41467-023-41721-9

Hörger AC, van der Hoorn RA. The structural basis of specific protease–inhibitor interactions at the plant–pathogen interface. *Curr Opin Struct Biol*. 2013:23(6):842–850. https://doi.org/10.1016/j.sbi.2013.07.013

Hörger AC, Ilyas M, Stephan W, Tellier A, van der Hoorn RAL, Rose LE. Balancing selection at the tomato *Rcr3* guardee gene family maintains variation in strength of pathogen defense. *PLoS Genet*. 2012:8(7):e1002813. https://doi.org/10.1371/journal.pgen.1002813

Ilyas M, Hörger AC, Bozkurt TO, van den Burg HA, Kaschani F, Kaiser M, Belhaj K, Smoker M, Joosten MHAJ, Kamoun S, et al. Functional divergence of two secreted immune proteases of tomato. *Curr Biol*. 2015:25(17):2300–2306. https://doi.org/10.1016/j.cub.2015.07.030

Jumper J, Evans R, Pritzel A, Green T, Figurnov M, Ronneberger O, Tunyasuvunakool K, Bates R, Žídek A, Potapenko A, et al. Highly accurate protein structure prediction with AlphaFold. *Nature*. 2021:596(7873):583–589. https://doi.org/10.1038/s41586-021-03819-2

Kaschani F, Shabab M, Bozkurt T, Shindo T, Schornack S, Gu C, Ilyas M, Win J, Kamoun S, van der Hoorn RAL. An effector-targeted protease contributes to defense against *Phytophthora infestans* and is under diversifying selection in natural hosts. *Plant Physiol*. 2010:154(4):1794–1804. https://doi.org/10.1104/pp.110.158030

Kim SH, Qi D, Ashfield T, Helm M, Innes RW. Using decoys to expand the recognition specificity of a plant disease resistance protein. *Science*. 2016:351(6274):684–687. https://doi.org/10.1126/science.aad3436

Kourelis J, Contreras MP, Harant A, Pai H, Lüdke D, Adachi H, Derevnina L, Wu C-H, Kamoun S. The helper NLR immune protein NRC3 mediates the hypersensitive cell death caused by the cell-surface receptor Cf-4. *PLoS Genet*. 2022:18(9):e1010414. https://doi.org/10.1371/journal.pgen.1010414

Kourelis J, Malik S, Mattinson O, Krauter S, Kahlon PS, Paulus JK, van der Hoorn RAL. Evolution of a guarded decoy protease and its receptor in solanaceous plants. *Nat Commun*. 2020:11(1):4393. https://doi.org/10.1038/s41467-020-18069-5

Krüger J, Thomas CM, Golstein C, Dixon MS, Smoker M, Tang S, Mulder L, Jones JDG. A tomato cysteine protease required for *Cf-2*-dependent disease resistance and suppression of autonecrosis. *Science*. 2002:296(5568):744–747. https://doi.org/10.1126/science.1069288

Laflamme B, Dillon MM, Martel A, Almeida RND, Desveaux D, Guttman DS. The pan-genome effector-triggered immunity landscape of a host-pathogen interaction. *Science*. 2020:367(6479):763–768. https://doi.org/10.1126/science.aax4079

Lewis JD, Lee AH-Y, Hassan JA, Wan J, Hurley B, Jhingree JR, Wang PW, Lo T, Youn JY, Guttman DS, et al. The *Arabidopsis* ZED1 pseudokinase is required for ZAR1-mediated immunity induced by the *Pseudomonas syringae* type III effector HopZ1a. *Proc Natl Acad Sci U S A*. 2013:110(46):18722–18727. https://doi.org/10.1073/pnas.1315520110

Lozano-Torres JL, Wilbers RHP, Gawronski P, Boshoven JC, Finkers-Tomczak A, Cordewener JH, America AH, Overmars HA, Van't Klooster JW, Baranowski L, et al. Dual disease resistance mediated by the immune receptor Cf-2 in tomato requires a common virulence target of a fungus and a nematode. *Proc Natl Acad Sci U S A*. 2012:109(25):10119–10124. https://doi.org/10.1073/pnas.1202867109

Luderer R, Takken FLW, de Wit PJGM, Joosten MHAJ. *Cladosporium fulvum* overcomes *Cf-2*-mediated resistance by producing truncated AVR2 elicitor proteins. *Mol Microbiol*. 2002:45(3):875–884. https://doi.org/10.1046/j.1365-2958.2002.03060.x

MacLean D. (2020). besthr - Generating bootstrap estimation distributions of HR data. https://doi.org/10.5281/zenodo.3374507

Martel A, Laflamme B, Seto D, Bastedo DP, Dillon MM, Almeida RND, Guttman DS, Desveaux D. Immunodiversity of the *Arabidopsis* ZAR1 NLR is conveyed by receptor-like cytoplasmic kinase sensors. *Front Plant Sci*. 2020:11:1290. https://doi.org/10.3389/fpls.2020.01290

Misas-Villamil JC, van der Hoorn RAL, Doehlemann G. Papain-like cysteine proteases as hubs in plant immunity. *New Phytol*. 2016:212(4):902–907. https://doi.org/10.1111/nph.14117

Mueller AN, Ziemann S, Treitschke S, Aßmann D, Doehlemann G. Compatibility in the *Ustilago maydis*–maize interaction requires inhibition of host cysteine proteases by the fungal effector Pit2. *PLoS Pathog*. 2013:9(2):e1003177. https://doi.org/10.1371/journal.ppat.1003177

Paulus JK, Kourelis J, Ramasubramanian S, Homma F, Godson A, Hörger AC, Hong TN, Krahn D, Ossorio Carballo L, Wang S, et al. Extracellular proteolytic cascade in tomato activates immune protease Rcr3. *Proc Natl Acad Sci U S A*. 2020:117(29):17409–17417. https://doi.org/10.1073/pnas.1921101117

Pérez-López E, Hossain MM, Wei Y, Todd CD, Bonham-Smith PC. A clubroot pathogen effector targets cruciferous cysteine proteases to suppress plant immunity. *Virulence*. 2021:12(1):2327–2340. https://doi.org/10.1080/21505594.2021.1968684

Pink M, Verma N, Rettenmeier AW, Schmitz-Spanke S. CBB staining protocol with higher sensitivity and mass spectrometric compatibility. *Electrophoresis*. 2010:31(4):593–598. https://doi.org/10.1002/elps.200900481

Postma J, Liebrand TWH, Bi G, Evrard A, Bye RR, Mbengue M, Kuhn H, Joosten MHAJ, Robatzek S. Avr4 promotes Cf-4 receptor-like protein association with the BAK1/SERK3 receptor-like kinase to initiate receptor endocytosis and plant immunity. *New Phytol*. 2016:210(2):627–642. https://doi.org/10.1111/nph.13802

Pottinger SE, Bak A, Margets A, Helm M, Tang L, Casteel C, Innes RW. Optimizing the PBS1 decoy system to confer resistance to potyvirus infection in *Arabidopsis* and soybean. *Mol Plant Microbe Interact*. 2020:33(7):932–944. https://doi.org/10.1094/MPMI-07-19-0190-R

Richau KH, Kaschani F, Verdoes M, Pansuriya TC, Niessen S, Stüber K, Colby T, Overkleeft HS, Bogyo M, van der Hoorn RAL. Subclassification and biochemical analysis of plant papain-like cysteine proteases displays subfamily-specific characteristics. *Plant Physiol*. 2012:158(4):1583–1599. https://doi.org/10.1104/pp.112.194001

Rooney HCE, Klooster JW, van't Hoorn RAL, van der Joosten MHAJ, Jones JDG, de Wit PJGM. *Cladosporium* Avr2 inhibits tomato Rcr3 protease required for *Cf-2*-dependent disease resistance. *Science*. 2005:308(5729):1783–1786. https://doi.org/10.1126/science.1111404

Schultink A, Qi T, Bally J, Staskawicz B. Using forward genetics in *Nicotiana benthamiana* to uncover the immune signaling pathway mediating recognition of the *Xanthomonas perforans* effector XopJ4. *New Phytol*. 2019:221(2):1001–1009. https://doi.org/10.1111/nph.15411

Schuster M, Eisele S, Armas-Egas L, Kessenbrock T, Kourelis J, Kaiser M, van der Hoorn RAL. Enhanced late blight resistance by engineering an EpiC2B-insensitive immune protease. *Plant Biotechnol J*. 2024:22(2):284–286. https://doi.org/10.1111/pbi.14209

Schuster M, Paulus JK, Kourelis J, van der Hoorn RAL. Purification of his-tagged proteases from the apoplast of agroinfiltrated *N. benthamiana*. In plant proteases and plant cell death: methods and protocols. In: Klemenčič M, Stael S, Huesgen PF, editors. *Methods in mol. Biol*. eds. New York, NY: Springer US; 2022. p. 53–66.

Seto D, Koulena N, Lo T, Menna A, Guttman DS, Desveaux D. Expanded type III effector recognition by the ZAR1 NLR protein using ZED1-related kinases. *Nat Plants*. 2017:3(4):17027. https://doi.org/10.1038/nplants.2017.27

Shabab M, Shindo T, Gu C, Kaschani F, Pansuriya T, Chintha R, Harzen A, Colby T, Kamoun S, van der Hoorn RAL. Fungal effector protein AVR2 targets diversifying defense-related cys proteases of tomato. *Plant Cell*. 2008:20(4):1169–1183. https://doi.org/10.1105/tpc.107.056325

Shindo T, van der Hoorn RAL. Papain-like cysteine proteases: key players at molecular battlefields employed by both plants and their invaders. *Mol Plant Pathol*. 2008:9(1):119–125. https://doi.org/10.1111/j.1364-3703.2007.00439.x

Shindo T, Kaschani F, Yang F, Kovács J, Tian F, Kourelis J, Hong TN, Colby T, Shabab M, Chawla R, et al. Screen of non-annotated small secreted proteins of *Pseudomonas syringae* reveals a virulence factor that inhibits tomato immune proteases. *PLoS Pathog*. 2016:12(9):e1005874. https://doi.org/10.1371/journal.ppat.1005874

Song J, Win J, Tian M, Schornack S, Kaschani F, Ilyas M, van der Hoorn RAL, Kamoun S. Apoplastic effectors secreted by two unrelated eukaryotic plant pathogens target the tomato defense protease Rcr3. *Proc Natl Acad Sci U S A*. 2009:106(5):1654–1659. https://doi.org/10.1073/pnas.0809201106

Tian M, Win J, Song J, van der Hoorn R, van der Knaap E, Kamoun S. A *Phytophthora infestans* cystatin-like protein targets a novel tomato papain-like apoplastic protease. *Plant Physiol*. 2007:143(1):364–377. https://doi.org/10.1104/pp.106.090050

Tyanova S, Temu T, Cox J. The MaxQuant computational platform for mass spectrometry-based shotgun proteomics. *Nat Protocols*. 2016:11(12):2301–2319. https://doi.org/10.1038/nprot.2016.136

van der Biezen EA, Jones JDG. Plant disease-resistance proteins and the gene-for-gene concept. *Trends Biochem Sci*. 1998:23(12):454–456. https://doi.org/10.1016/S0968-0004(98)01311-5

van der Hoorn RAL, Kamoun S. From guard to decoy: a new model for perception of plant pathogen effectors. *Plant Cell*. 2008:20(8):2009–2017. https://doi.org/10.1105/tpc.108.060194

van der Hoorn RAL, de Wit PJGM, Joosten MHAJ. Balancing selection favors guarding resistance proteins. *Trends Plant Sci*. 2002:7(2):67–71. https://doi.org/10.1016/S1360-1385(01)02188-4

van der Hoorn RAL, Laurent F, Roth R, de Wit PJGM. Agroinfiltration is a versatile tool that facilitates comparative analyses of *Avr9/Cf-9*-induced and *Avr4/Cf-4*-induced necrosis. *Mol Plant Microbe Interact*. 2000:13(4):439–446. https://doi.org/10.1094/MPMI.2000.13.4.439

van't Klooster JW, van Der Kamp MW, Vervoort J, Beekwilder J, Boeren S, Joosten MHAJ, Thomma BPHJ, de Wit PJGM. Affinity of Avr2 for tomato cysteine protease Rcr3 correlates with the Avr2-triggered *Cf-2*-mediated hypersensitive response. *Mol Plant Pathol*. 2011:12(1):21–30. https://doi.org/10.1111/j.1364-3703.2010.00647.x

Wang G, Roux B, Feng F, Guy E, Li L, Li N, Zhang X, Lautier M, Jardinaud M-F, Chabannes M, et al. The decoy substrate of a pathogen effector and a pseudokinase specify pathogen-induced modified-self recognition and immunity in plants. *Cell Host Microbe*. 2015:18(3):285–295. https://doi.org/10.1016/j.chom.2015.08.004

Weber E, Engler C, Gruetzner R, Werner S, Marillonnet S. A modular cloning system for standardized assembly of multigene constructs. *PLoS One*. 2011:6(2):e16765. https://doi.org/10.1371/journal.pone.0016765

Yu Y, Tang W, Lin W, Li W, Zhou X, Li Y, Chen R, Zheng R, Qin G, Cao W, et al. ABLs and TMKs are co-receptors for extracellular auxin. *Cell*. 2023:186(25):5457–5471.e17. https://doi.org/10.1016/j.cell.2023.10.017